ACS MATERIALS Au
AN OPEN ACCESS JOURNAL OF THE AMERICAN CHEMICAL SOCIETY

pubs.acs.org/materialsau

Review

Strategies for Controlled Growth of Transition Metal Dichalcogenides by Chemical Vapor Deposition for Integrated Electronics

Ting Kang,[§] Tsz Wing Tang,[§] Baojun Pan,[§] Hongwei Liu, Kenan Zhang, and Zhengtang Luo*

Cite This: *ACS Mater. Au* 2022, 2, 665−685

Read Online

ACCESS | Metrics & More | Article Recommendations

ABSTRACT: In recent years, transition metal dichalcogenide (TMD)-based electronics have experienced a prosperous stage of development, and some considerable applications include field-effect transistors, photodetectors, and light-emitting diodes. Chemical vapor deposition (CVD), a typical bottom-up approach for preparing 2D materials, is widely used to synthesize large-area 2D TMD films and is a promising method for mass production to implement them for practical applications. In this review, we investigate recent progress in controlled CVD growth of 2D TMDs, aiming for controlled nucleation and orientation, using various CVD strategies such as choice of precursors or substrates, process optimization, and system engineering. We then survey different patterning methods, such as surface patterning, metal precursor patterning, and postgrowth sulfurization/selenization/tellurization, to mass produce heterostructures for device applications. With these strategies, various well-designed architectures, such as wafer-scale single crystals, vertical and lateral heterostructures, patterned structures, and arrays, are achieved. In addition, we further discuss various electronics made from CVD-grown TMDs to demonstrate the diverse application scenarios. Finally, perspectives regarding the current challenges of controlled CVD growth of 2D TMDs are also suggested.

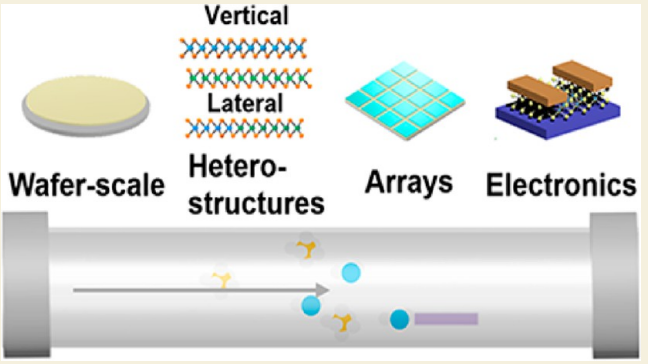

KEYWORDS: *transition metal dichalcogenides, chemical vapor deposition, wafer-scale, heterostructures, arrays, electronics*

1. INTRODUCTION

The study of two-dimensional (2D) van der Waals (vdW) materials represented by graphene is one of the most interesting research topics because of their extraordinary solid-state physics[1−4] and application potential for next-generation nanoelectronics.[5,6] However, graphene as a zero band gap semimetal fails to play a role as a semiconducting active channel in electronics. Transition metal dichalcogenides (TMDs), with a layered structure similar to that of graphene, complement this disadvantage. Previous research has extensively investigated group VIB TMDs such as MoS_2, $MoSe_2$, WS_2, $MoTe_2$, etc., in both fundamental research[7−11] and industry.[12−14] The majority of these group VIB TMDs are thermodynamically stable semiconductors with a sizable band gap and are commonly used as active channels in optoelectronics. In recent years, due to the development of producing technology, much research is also devoted to other novel TMDs. For instance, 2D ferromagnetism[15,16] and 2D ferroelectricity[17] have been found on VSe_2 and twisted TMDs, respectively. Due to its large family and diverse nature, TMDs are undoubtedly one of the most promising branches of two-dimensional vdW to realize versatile applications in various scenarios like optoelectronics,[18,19] electrocatalysis,[20] membrane filtration,[21] memories,[22] etc.

Many synthesis routes for 2D TMDs have been widely explored, including mechanical exfoliation, chemical exfoliation, molecular beam epitaxy (MBE), and chemical vapor deposition (CVD). Mechanical exfoliation operated with Scotch tape obtains samples with high crystallinity, cleanliness, low defects, and controllable thickness.[23] However, this manual operation obviously cannot meet the needs of large-scale production, thus it is rarely used outside of cutting-edge fundamental research. Chemical exfoliation, such as liquid exfoliation[24] and intercalation exfoliation,[25] weakens the interlayer vdW force of TMDs by polar molecules or ions to exfoliate bulk TMDs to few-layer equivalents using a top-down

Received: April 19, 2022
Revised: June 23, 2022
Accepted: June 24, 2022
Published: July 8, 2022

https://doi.org/10.1021/acsmaterialsau.2c00029
ACS Mater. Au 2022, 2, 665−685

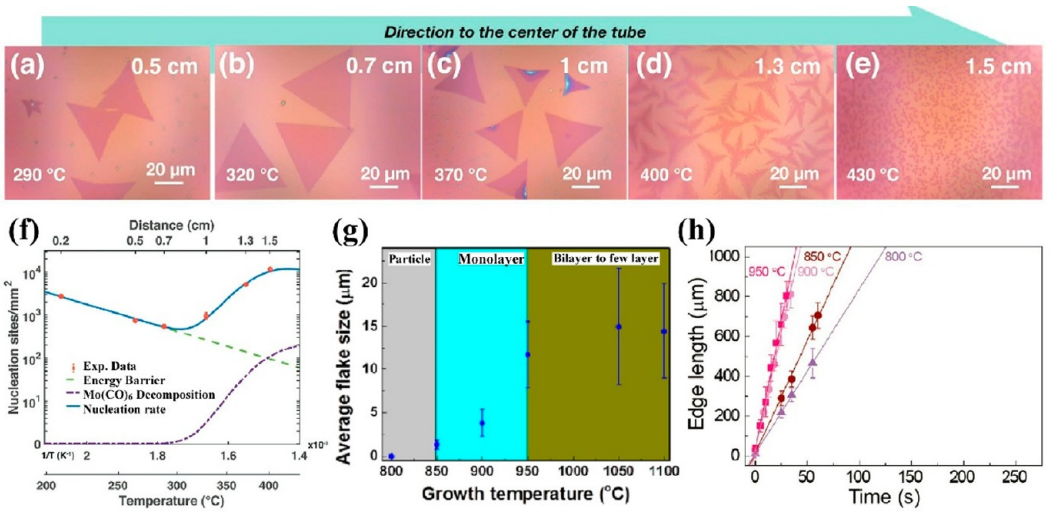

Figure 1. Thermodynamics and kinetics in CVD growth of TMDs. (a–e) Optical images of monolayer MoS_2 with growth temperature from 290 to 430 °C and growth time of 6 h. (f) Evolution of nucleation density of CVD-grown MoS_2 with temperatures. Reprinted with permission from ref 40. Copyright 2021 Wiley-VCH. (g) Relationship between average flake size and growth temperature of monolayer WSe_2, showing suppressed nucleation density with high temperature. Reprinted from ref 41. Copyright 2015 American Chemical Society. (h) Plot of edge length of WSe_2 against time, showing the growth rate is affected by temperature-dependent partial pressure of the precursors. Reprinted with permission from ref 45. Copyright 2017 Wiley-VCH. The temperature and partial pressure as parameters jointly affect the nucleation and growth in the CVD process of TMDs.

method. Although mass production is achievable by chemical exfoliation, limited surface area, poor controllability, and toxicity remain challenges of this approach. CVD, the most representative "bottom-up" method, is perhaps the most promising route among these for efficient production. The CVD growth of TMDs still obeys classical nucleation theory (CNT)[26] and is mainly divided into two stages, nucleation and growth. Therefore, by reasonably controlling the growth conditions of the crystals, the synthesis of large-sized high-quality TMD thin films is completely possible by CVD. However, the controllable CVD growth of 2D TMDs is still a huge challenge, despite nearly 10 years of development. The main reason is that the CVD process involves a series of complex chain chemical reactions involving vapors and also involves complicated interactions between the vapor precursors, formed crystals, and the substrate. Generally, the CVD process is extremely sensitive to the local environment in the reaction chamber, and thus most studies related to the controllable CVD growth are based on experimental results, supplemented by an explanation of the mechanisms, although computational simulations related to it have only been preliminarily explored so far.[27−29] In this regard, we review the recent works reporting the synthesis of 2D TMDs and 2D TMD heterostructures, with a focus on the strategies made to achieve a high degree of growth controllability via the CVD method. In addition, mechanistic insights are also provided to understand the chemistry in the controllable CVD growth. To better understand the necessity and significance of synthesizing 2D TMDs, the structure and properties of 2D TMDs are introduced first. Then several of the most common types of CVD are discussed, with a focus on how to achieve controllable growth of pure TMDs by choosing and designing precursors or substrates. To further illustrate the advantage of CVD for controlled synthesis, the growth of more complex products such as TMD heterostructures and patterned TMD arrays are presented, involving various technologies, smart strategies, and design routes. At the end of this review, a brief summary of the CVD-grown TMD applications is presented to better understand what practical use can be achieved by controlled CVD growth.

2. STRUCTURE AND PROPERTIES OF 2D TMDs

Transition metal dichalcogenides have structures adopting the MX_2 formula, where M and X refer to transition metal atoms (M = Mo, W, Nb, V, Re, Ta, etc.) and chalcogen atoms (X = S, Se, Te) separately. Unlike graphene, which is composed of only carbon atoms in a plane, TMDs have a sandwich structure with chalcogen atoms on top and bottom and are covalently bonded to transition metal atoms in the middle. According to the coordination, TMD monolayers are classified into 1H (trigonal prismatic) phase and 1T (octahedral) phase. Beyond basic 1H and 1T phases, polymorphs including 1T′ (distorted 1T), T_d (orthorhombic), 2H, and 3R are discovered. 1T′ and T_d are derivatives of 1T, and they differ from 1T in intralayer coordination between chalcogen atoms and transition metal atoms. 2H and 3R originate from multilayers stacked with 1H monolayers by ABA and ABC sequences,[30,31] respectively. Generally, phase transition leads to the change but is not the decisive factor in the electrical properties of TMDs. The most typical example is the phase transition of $MoTe_2$, from the metallic 1T′ phase to the semiconducting 2H phase.[32] The difference in electronic properties comes from the filling level of nonbonding d orbitals of transition metals. When no partially occupied nonbonding orbital exists, the TMD is semiconducting, e.g., 2H-WS_2 and 1T-PtS_2; otherwise, it is metallic like 1T-ReS_2 and 2H-TaS_2.[33] The phase of TMDs could be engineered by diverse approaches such as intercalation,[34] strain,[35] and thermal treatment.[32]

3. CONTROLLABLE CVD GROWTH OF TMDs

TMDs with wafer-scale size, uniform thickness, and high crystallinity are the main considerations for future material development, aiming for optimizing the fabrication and performance of electrical and optoelectronic devices. The

https://doi.org/10.1021/acsmaterialsau.2c00029
ACS Mater. Au 2022, 2, 665−685

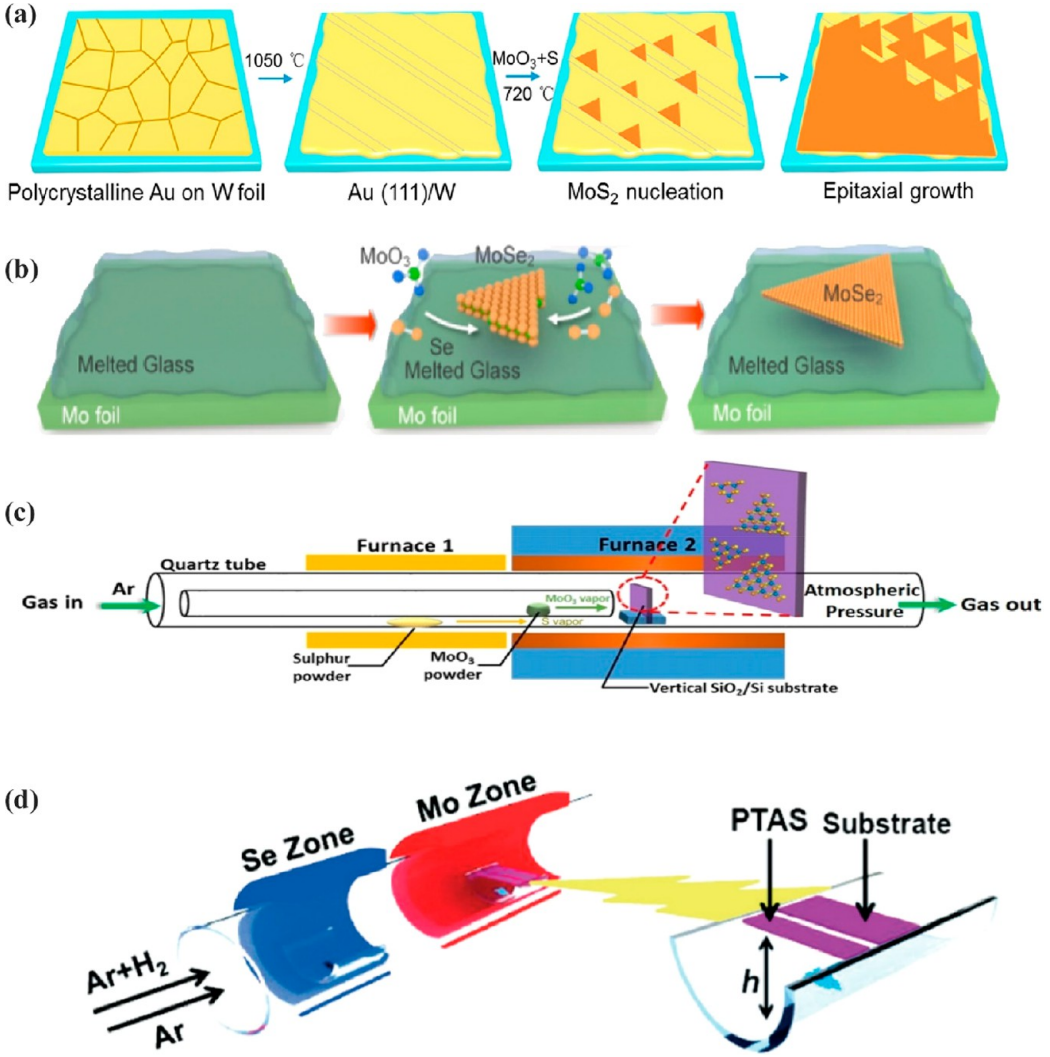

Figure 2. Controllable nucleation and epitaxial growth of TMDs via APCVD. (a) Evolution of wafer-scale unidirectional MoS_2 monolayer on a Au(111) substrate. Reprinted from ref 47. Copyright 2020 American Chemical Society. (b) Growth scheme of large-scale single-crystalline $MoSe_2$ on a molten glass substrate. Reprinted from ref 48. Copyright 2017 American Chemical Society. (c) Growth manner of MoS_2 film via substrate control. Reprinted with permission from ref 49. Copyright 2016 IOP Publishing Ltd. (d) Schematic illustration of the growth of $MoSe_2$ with the use of PTAS seed promoter. Reprinted with permission from ref 50. Copyright 2018 The Royal Society of Chemistry. Using a suitable substrate and adjusting the substrate locations and orientations, the morphology of the TMD grains can be effectively controlled.

morphology of the TMD films will be easily modified by the growth parameters, such as the type and structure of the substrate,[36] reaction temperature,[37] flow rate,[37] type of precursors,[38] etc. To reach the controllable CVD growth of wafer-scale, grain-boundary-free, and highly uniform TMDs, precise research should focus on atmospheric pressure CVD (APCVD), low-pressure CVD (LPCVD), and metal-organic CVD (MOCVD).

3.1. Thermodynamics and Kinetics in CVD Growth of TMDs

In CVD synthesis, very small change in parameters may largely vary the kinetics and thermodynamics of TMD growth, leading to drastic changes in the products. It is necessary to explore a deeper understanding of the kinetic and thermodynamic factors in the CVD growth mechanism of such 2D materials. The impact of thermodynamics and kinetics on the vapor deposition process is mainly reflected in two local parameters: (1) reaction temperature and (2) partial pressure around the substrate.

To date, thermodynamic and kinetic studies based on the gradient temperature growth of TMDs via the CVD mechanism have been explored.[26,39] Detailed thermodynamic and kinetic studies based on the CVD mechanism were performed and found that the crystal nucleation density significantly depends on the temperature.[40] This phenomenon can be explained by the classical nucleation theory.

$$N = AP(T)\exp\left(\frac{E_{des} - E_s - \Delta G^*}{kT}\right)$$

where N is the nucleation rate, T is the zone temperature, P is the partial pressure of the Mo species, E_{des} is the desorption energy for molecules back to the vapor phase, E_s is the activation energy for surface diffusion, and ΔG^* is the CNT free energy. The nucleation growth of monolayer MoS_2 in the low-temperature range, in which crystal nucleation density increased, is in contrast to the high-temperature range. For a high-temperature reaction, the partial pressure of the precursor is regarded as a constant due to almost complete sublimation,

https://doi.org/10.1021/acsmaterialsau.2c00029
ACS Mater. Au 2022, 2, 665−685

thus the nucleation rate is exclusively determined by temperature (Figure 1g).[41] The nucleation density undergoes inhibition as substrate temperature increases, whereas the supersaturation is satisfied.[42] In contrast, both partial pressure and temperature contribute to the nucleation rate and density and thus the grain size of MoS_2 at a relatively low temperature, due to the unsaturated local concentration of the precursor (Figure 1a–f).

The partial pressures of the vaporized solid precursors can be controlled by different approaches, such as gas flow rate adjustment,[42] zone temperature modification,[40] precursor concentration modulation,[43] etc., and different kinetic regimes exist, leading to the production of the desired TMD monolayers. For instance, the stable TMD crystal growth under thermodynamic and kinetic control can be balanced by an increasing gas flow rate, thus modifying the partial pressure of the transition metal source along the gas flow, and the result shows a strong dependence of TMDs' crystal growth rate on the precursors' partial pressure.[44] A study investigated the effect of precursor partial pressure on the MoS_2 growth rate and crystal domain shape and found that increasing the MoO_3 mass transfer under a high gas flow rate has an impact on the faster crystal growth rate and showed the influence on the kinetic growth dynamics of edges.[42] Moreover, the partial pressures of precursors depend on the temperature, which determines the decomposition and sublimation rates of the precursors. As shown in Figure 1h, faster W source supply can be achieved by increasing the growth temperature while ensuring sufficient Se feeding, leading to a higher growth rate of WSe_2.[45]

3.2. Atmospheric Pressure CVD

APCVD is a vapor deposition process under a normal pressure environment. The TMD materials were grown by delivering evaporated precursors, usually inorganic and less toxic, to the substrate surface.[46] The control of nucleation density, oriented growth, numbers of layers, crystal shapes, domain size, etc. is considered to be the major direction for desired TMD growth. In order to control the nucleation and oriented growth in APCVD, in addition to the parameters, such as temperature, airflow, etc., the main consideration is to select a proper substrate and its placement.

Recent research discussed the distribution of a suitable substrate in TMD growth by controlling desired nucleation density, orientation, and domain size. As shown in Figure 2a, the highly uniform, epitaxial wafer-scale, single-crystalline growth of a MoS_2 monolayer was obtained on a Au(111) substrate.[47] Gold foil was melted and resolidified on tungsten foil to obtain the single-crystalline Au(111) film and to produce unidirectional nucleation–growth of the single-crystalline MoS_2 wafer. Similarly, recent research achieved the production of millimeter-sized $MoSe_2$ crystals with high uniformity on a molten glass substrate.[48] An ultrasmooth and liquid-like isotropic surface was generated by increasing the temperature to 750 °C. The successful growth of a large domain crystalline $MoSe_2$ monolayer on the molten glass substrate is due to the suppression of nucleation (Figure 2b). As a result, the nucleation density reduction led to a large-sized crystalline TMD, illustrating the importance of a suitable substrate for the APCVD system.

Other than the substrate selection, the location, position, and orientations of the substrate also play an important role. The production of large-scale monolayer molybdenum disulfide film, up to centimeter scale, was achieved on the surface of a vertically positioned silicon substrate.[49] Unlike the horizontal substrate, the vertical substrate enables uniform seeding of the MoO_3 precursor on the substrate (Figure 2c). The position height between the substrate and the precursor is another key factor in the APCVD system that determines nucleation density and shape. The growth of different types of $MoSe_2$ nanosheets, including two-dimensional triangle domains, hexagons, three-dimensional pyramids, and vertically aligned grains, was achieved. The CVD growth of $MoSe_2$ was processed at 750 °C with the help of a seed promoter (tetrapotassium perylene-3,4,9,10-tetracarboxylate). The tailored morphologies were achieved by adjusting the height between the silicon substrate and solid precursor, resulting in the production of differently shaped TMDs (Figure 2d).[50] Moreover, the role of distance between the precursor source and substrate in CVD morphology was also shown to be vital. Another TMD shape-controlling method, by varying the spatial locations of the silicon substrates in the furnace tube, was reported,[42] and it found that the shape of the MoS_2 domain was highly associated with the locations of the SiO_2/Si substrate. The shape of MoS_2 changed from triangular to hexagonal when the distance from the substrate away from the MoO_3 powder was varied. Compared to the silicon substrate, recent research showed a significant development in domain size and uniformity of TMD films using other types of substrates. Further development of the APCVD engineering system to fabricate the TMD materials with better uniformity and quality is still highly desired. APCVD is the most widely explored CVD technique and has potential for the development of high efficiency, simple setup, and low-cost 2D TMD film fabrication with large-scale and high uniformity. However, the sulfurization and selenization process requires a high growth temperature of greater than 750 °C, where the high processing temperature limited the use of some specific substrates,[51] like polymeric substrates. The melting temperature of many polymeric substrates, such as polyamide, was below the CVD processing temperature of TMD synthesis.[52] The additional transfer is necessary and thus limits the applications of polymeric films in TMD flexible devices.

3.3. Low-Pressure CVD

LPCVD growth of TMD films is processed under a low-pressure environment. Lower pressure can reduce unnecessary gas-phase reactions, leading to the increase of the uniformity of TMD films on the wafer.[53] As the domain size of TMDs is highly related to the nucleation density, the concentration of precursors and the type of substrates are the noteworthy factors to control the nucleation, to enable epitaxial growth, and to eliminate the grain boundaries of CVD-grown TMDs. Based on the recent development of LPCVD synthesis technology, the growth of large domain size single-crystalline TMDs with limited grain boundary films can be obtained.

In LPCVD, the selection of a suitable pretreated substrate still plays a significant role in the synthesis of TMDs with controlled domain orientation and alignment. Many research groups discovered that the use of suitable single-crystalline substrates, such as a-plane sapphire,[54] c-plane sapphire,[55] GaN,[56] etc., is the key factor in the growth of satisfactory oriented and aligned TMD films. A dual-coupling-guided epitaxy growth of WS_2 on a step-edged a-plane sapphire under a 300 Pa Ar atmosphere demonstrated the formation of large-sized single-crystalline WS_2 grains with unidirectional align-

https://doi.org/10.1021/acsmaterialsau.2c00029
ACS Mater. Au 2022, 2, 665–685

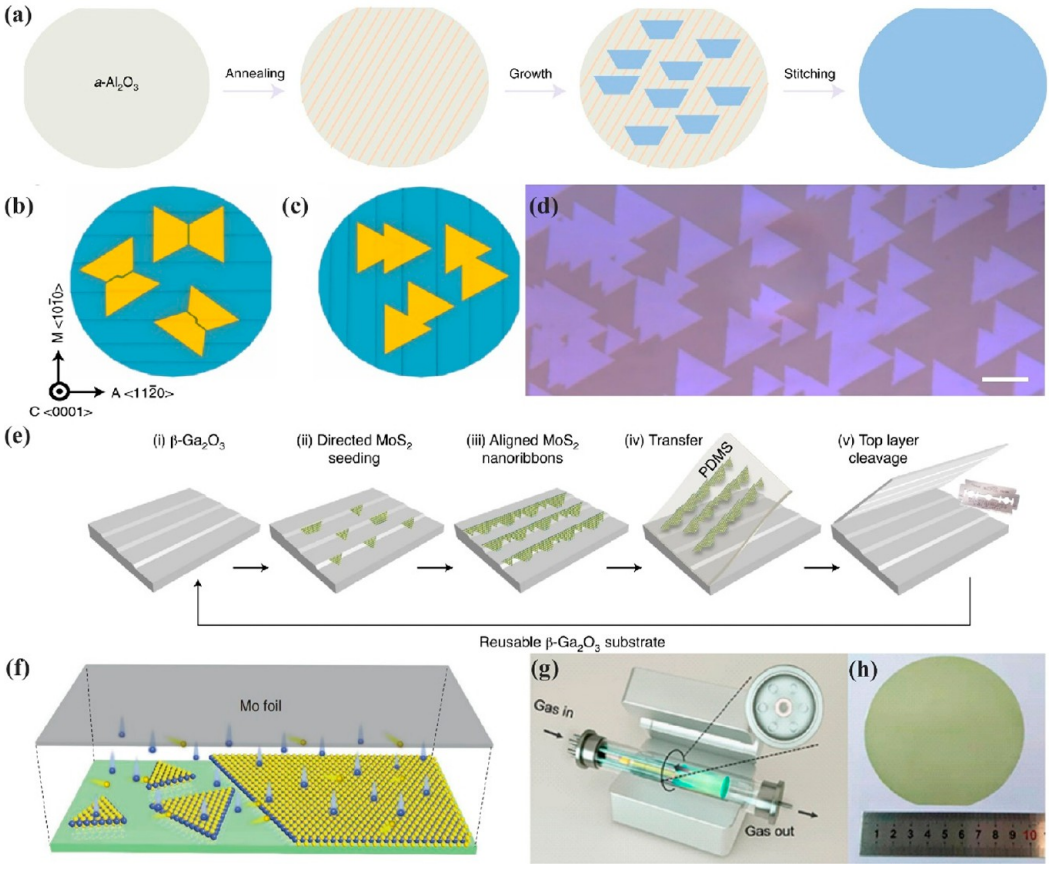

Figure 3. Controllable nucleation and oriented growth of TMDs via LPCVD. (a) Schematic of the CVD processing of large-size unidirectionally aligned WS_2 on step-edged a-plane sapphire. Reprinted with permission from ref 54. Copyright 2022 Springer Nature. Schematic of MoS_2 domains growth on (b) C/M and (c) C/A sapphire and (d) optical image of MoS_2 monolayer growth in step-edged C/A sapphire. Reprinted with permission from ref 55. Copyright 2021 Springer Nature. (e) Schematic of the self-aligned growth of continuous MoS_2 nanoribbons on β-gallium(III) oxide substrate. Reprinted with permission from ref 57. Copyright 2020 Springer Nature. (f) Schematic diagram of the face-to-face precursors feeding LPCVD growth of MoS_2 on the soda-lime glass substrate. Reprinted with permission from ref 58. Copyright 2018 Springer Nature, open access. (g) Schematic diagram of multisource CVD system for large-size MoS_2 kinetic controllable LPCVD growth. (h) Optical image of wafer-scale (4 in.) monolayer MoS_2. Reprinted from ref 60. Copyright 2020 American Chemical Society. The controllable nucleation and oriented LPCVD growth were developed by the use of suitable substrates and reaction programming, leading to the improvement in uniformity and quality of TMD films.

ment and seamless stitching.[54] They found that the epitaxial stitching of WS_2 on the substrate of a-plane Al_2O_3 depends on the dual-coupling-guided mechanism, and the theoretical calculation was analyzed by density functional theory (DFT). Due to the coupling between WS_2 grains and a-plane Al_2O_3 and the coupling between WS_2 and a step-edged substrate, unidirectional alignment of WS_2 with a 2 in. single-crystalline monolayer was achieved (Figure 3a). Similarly, another report demonstrated the TMDs' epitaxial growth of unidirectionally aligned MoS_2 single crystals on step-edged c-plane sapphire (0001) under the LPCVD processing system.[55] The orientation of step-edging was perpendicular to the standard sapphire substrate, and MoS_2 was grown on the C/A α_A = 0.89° sapphire substrate (Figure 3b–d). Using another single-crystalline substrate, β-Ga_2O_3 film, a controlled MoS_2 growth via ledge-directed epitaxy-assisted chemical vapor deposition processing under 30 Torr was achieved.[57] The single-crystalline monolayer MoS_2 was formed as a high-quality nanoribbon with continuous arrays and aligned orientation. It is demonstrated that the nucleation of MoS_2 occurred at the ledges of the β-gallium(III) oxide substrate, followed by the merging of an aligned MoS_2 domain, and the synthesis of self-aligned continuous nanoribbons was achieved ultimately (Figure 3e).

Apart from the oriented growth, a suitable substrate efficiently determines nucleation density, similar to APCVD growth. Batch production of MoS_2 is demonstrated by an efficient growth of MoS_2 by face-to-face precursor feeding.[58] Using soda-lime glass as the substrate and oversaturated S precursor, the evaporation of Mo source can be limited and fabricate large domain size 6 in. MoS_2 (Figure 3f). It is concluded that selecting a suitable substrate controls the nucleation density, and the single-crystalline substrate with the pretreated surface can promote the oriented and aligned growth of high uniformity TMDs.[59]

Moreover, the growth of TMDs with high uniformity and large size can be obtained by modulation of the reaction system, e.g., process optimization, and system engineering. The production of high-quality and large domain size monolayer MoS_2 film on the sapphire wafers by multisource system design of LPCVD was reported.[60] To ensure steady evaporation, the multipocket sources were designed to achieve facile evaporation of precursors and growth of TMD films. As shown in Figure 3g,h, S and MoO_3 sources were loaded in several inner-

https://doi.org/10.1021/acsmaterialsau.2c00029
ACS Mater. Au 2022, 2, 665–685

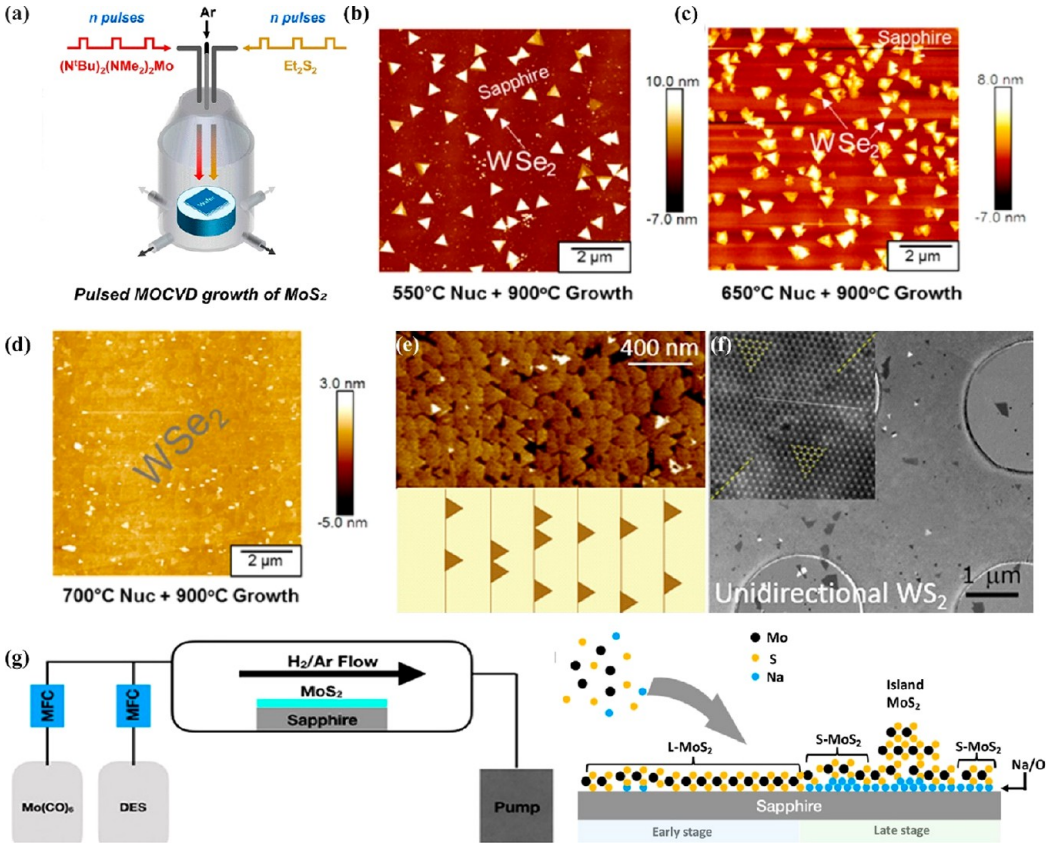

Figure 4. Controllable lateral epitaxial growth of TMDs via MOCVD. (a) Overview of the pulsed MOCVD processing design for thickness-controlled MoS_2 growth. Reprinted from ref 66. Copyright 2017 American Chemical Society. (b) AFM scan of WSe_2 film on the scale of 1−2 μm without a nucleation step (low density and coverage). (c,d) AFM scan of WSe_2 film with nucleation and growth steps, showing an increase in density and coverage with different temperatures. Reprinted with permission from ref 67. Copyright 2016 IOP Publishing Ltd. (e) Schematic of the top view of the substrate with unidirectional WS_2 domains. (f) Composite dark-field TEM image and the inset with higher resolution confirms well-aligned crystal orientation. Reprinted from ref 69. Copyright 2021 American Chemical Society. (g) Schematic of the MOCVD reactors shows the sapphire in a hot-wall tube reactor and hypothesized mechanism of NaCl-assisted growth of early stage and late stage. Reprinted from ref 68. Copyright 2018 American Chemical Society. In order to obtain the wafer-size and high-uniformity TMD films, the MOCVD growth was developed by the use of suitable precursors and well-designed growth programming and processing steps.

miniature quartz tubes to achieve the precise kinetic control for the growth of single-crystalline MoS_2. To control the nucleation density by adjusting the precursor concentration,[61] a partial pressure programming LPCVD system was reported.[62] The concentration and distribution were controlled by changing the amount of solid MoO_3 and the height between substrate and precursor. By controlling the flux of the Mo species, a reaction transition for MoS_2 growth was achieved, and the MoS_2 crystal was changed from a gradient-distributed triangular shape to a large-sized continuous monolayer. The vitality of metal precursors in the LPCVD-growth system was well-proven due to its role in controlling the layer number and thickness uniformity.

The low processing pressure leads to the improvement in the uniformity and purity of the produced TMD films. In contrast to APCVD, LPCVD is able to reduce the rate of gas-phase prereaction and film deposition and thus facilitates the TMD synthesis with better quality and uniformity and has the potential to produce a large-scale continuous film.[62] Nevertheless, for growth control of wafer-sized TMD films, from isolated domains to a large continuous film, the systematic understanding of the growth mechanism is still not clear.[63] The commercial purposes of the semiconductor industry prefer the high uniformity and continuous films up to wafer-scale, but most LPCVD-grown TMDs still cannot meet the requirement. The controllable LPCVD fabrication of high uniformity and wafer-scale TMD films is still a key challenge and prospective direction in further research. In addition, the high processing temperature of the LPCVD system also limits the use of low melting temperature substrates.

3.4. Metal-Organic CVD

MOCVD is the CVD technology that uses organic metals, such as metallocene complexes, metal carbonyls, cyclopentadienyl ligands, etc., as the precursors.[64] The nucleation, epitaxial growth, and control of film thickness are the major prospective directions in recent MOCVD research that contribute to the improvement of coverage and quality of TMD films.[65] To control the lateral epitaxial growth in the MOCVD system, the precursor and the process must be designed elaborately.

The variety of precursors directly correlates with the concentration of metal source and chalcogen source and results in the varying of morphology, lateral growth, and quality of the films. A recent report demonstrated the production of few-layered MoS_2 growth by a pulsed MOCVD system with the use of bis(*tert*-butylimido)bis-(dimethylamindo)molybdenum [$(NtBu)_2(NMe_2)_2Mo$] and diethyl disulfide (Et_2S_2) as the precursors.[66] To achieve thickness control of the MoS_2 film, the deposition process was

https://doi.org/10.1021/acsmaterialsau.2c00029
ACS Mater. Au 2022, 2, 665−685

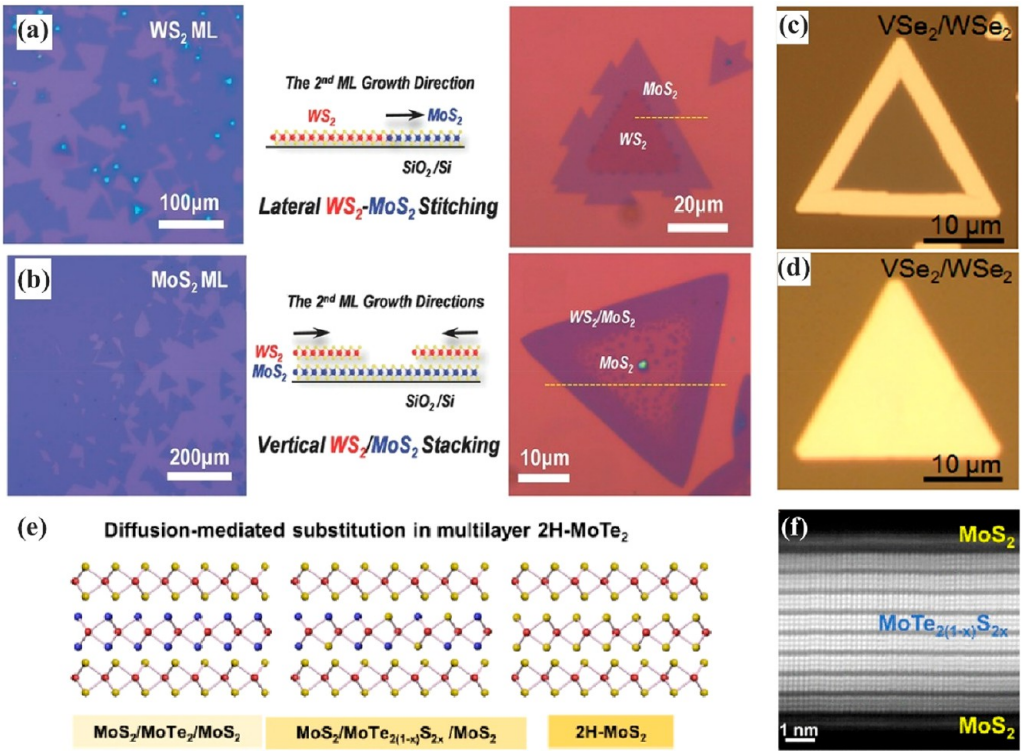

Figure 5. Controllable growth path of vertical TMD heterostructures. Growth mode of (a) WS_2−MoS_2 using WS_2−MoS_2 growth sequence and (b) WS_2/MoS_2 using MoS_2−WS_2 growth sequence, with the optical images. Reprinted with permission from ref 93. Copyright 2015 Wiley-VCH. Optical images of (c) partially covered and (d) fully covered VSe_2/WSe_2. Reprinted from ref 96. Copyright 2019 American Chemical Society. (e) Schematic illustration of substitution of sulfur to multilayer 2H-$MoTe_2$. (f) Cross-sectional STEM image of symmetrical MoS_2/$MoTe_{2(1-x)}S_{2x}$/MoS_2. Reprinted from ref 99. Copyright 2021 American Chemical Society. The two-step method is the main CVD method to obtain vertical heterobilayer and the top layer usually starts their growth from the edge of the bottom. Other ways such as chalcogen substitution also enable the preparation of vertical heterostructures.

conducted by several precursor injections (n = 0, 15, 50, 100) and resulted in the achievement of 1−25 nm MoS_2 film in a very short deposition time (Figure 4a). Apart from the selection of precursors, the precursor flow ratio also plays a role in the MOCVD system. The synthesis of WSe_2 films with outstanding improvement in surface coverage, thickness uniformity, and crystalline quality was reported.[67] The extreme precursor ratio of $(CH_3)_2Se/W(CO)_6$ was set at 14000, and the lateral growth and nucleation of the TMD were controlled, resulting in the fabrication of high uniformity films (Figure 4b−d).

The important role of alkali-assisted precursors in CVD processing is also demonstrated, which leads to the impacts in growth morphology, including growth rate, loss of epitaxy, nucleation density, etc. Production of two-dimensional TMD films with a large domain size and fully coalesced polycrystalline structure was successfully achieved.[68] The MoS_2 film was synthesized in the MOCVD hot-wall tube reactor using $Mo(CO)_6$ and DES as the metal and chalcogen precursors with the utilization of alkali salts, such as sodium chloride and potassium iodide. Comparing the epitaxial growth of MoS_2 under alkali-free growth and alkali-assisted growth, the dramatic increase in the domain size of the MoS_2 monolayer by ∼20-fold was achieved by NaCl alkali-assisted growth. However, the alkali-assisted growth led to the saturation of Na−O bonding on the substrate surface and resulted in the reduction of substrate surface energy, weakening of the epitaxial growth, and the occurrence of multilayered MoS_2 film (Figure 4g).

In order to control the epitaxial growth of TMD films in the MOCVD system, modifying the reaction process is also important to promote large-scale TMD films. A production of large-scale single-crystalline WS_2 continuous monolayer films with control of epitaxial growth and stitching of the oriented domains was realized.[69] With the use of a variable-temperature multistep process, the coalesced unidirectional WS_2 film grew on the 2 in. diameter c-plane sapphire by MOCVD. With the help of multistep programming, control of the surface diffusion, epitaxial domain growth, and self-stitching of domain growth were achieved (Figure 4e,f).

In addition to the controlled epitaxial growth, the TMD growth on the selective area can also be achieved using the well-designed processing treatment. A recent report demonstrated a method for controlling the TMD lateral growth on desired regions by a seed-free, site-specific nucleation MOCVD.[70] In order to achieve the selective area growth of TMDs, a multistep surface functionalization approach was developed. The polymer functional layer was formed by the conventional lithographic process, and the sapphire surface is used as the original photoresist mask, followed by MOCVD growth at 825 °C. A route for the controlled TMD growth with exact patterns was demonstrated, and the device performance of the TMD film is comparable to that of the film produced by mechanical exfoliation.

The MOCVD method provides a new approach for manufacturing TMD films with a faster deposition rate. The significant advantages of MOCVD are its capability for large-scale TMD film fabrication with excellent conformal coverage

https://doi.org/10.1021/acsmaterialsau.2c00029
ACS Mater. Au 2022, 2, 665−685

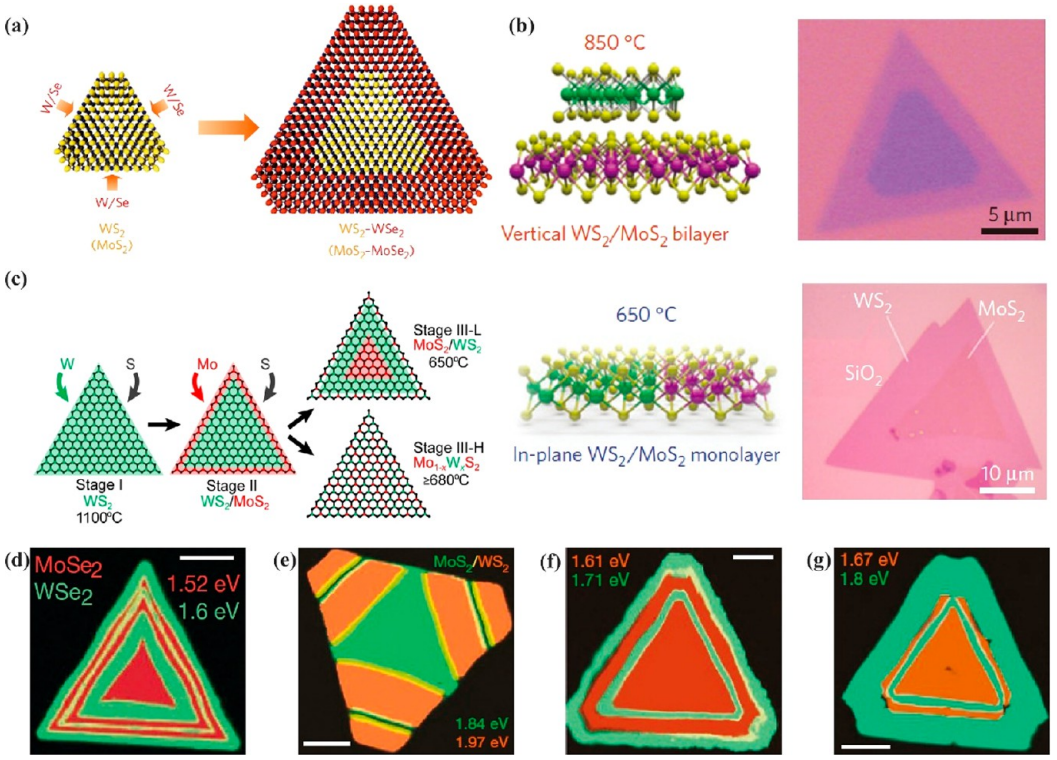

Figure 6. Controllable growth path of lateral TMDs heterostructures. (a) Illustration of in-plane epitaxy of MS_2−MSe_2 (M = Mo or W) in one-pot growth. Reprinted with permission from ref 105. Copyright 2014 Springer Nature. (b) Growth-temperature-dependent architecture of heterostructure based on WS_2 and MoS_2. Reprinted with permission from ref 102. Copyright 2014 Springer Nature. (c) Reconstruction of edge epitaxy in WS_2−$MoSe_2$, influenced by temperature. Reprinted from ref 106. Copyright 2016 American Chemical Society. PL mapping of $MoSe_2$−WSe_2 (d), $MoSe_2$−WS_2 (e), and $MoS_{2(1-x)}Se_{2x}$−$WS_{2(1-y)}Se_{2y}$ (f,g). Reprinted with permission from ref 110. Copyright 2018 Springer Nature. To synthesize in-plane TMD heterojunctions with aimed core-ring structure, the control of temperature and vapor sources is significant.

and its ability to synthesize new metastable materials, including oxide,[71] carbides,[72] silicide,[73] etc. MOCVD also showed the potential for versatile TMD growth under relatively low temperatures[40,74] and its ability to promote the use of a wide range of low melting temperature substrates, including polymeric film. However, it is worth noting that the organic metal precursors and other reaction sources are usually highly toxic. Apart from the toxic precursors, the deposition process will also lead to the emission of highly hazardous exhaust gas, such as arsine, phosphine, etc. The low production rate, high production cost, and toxic organic precursors limit its application and prohibit its development.

4. CONTROLLABLE CVD GROWTH OF TMD HETEROSTRUCTURES

The conventional transfer method cannot satisfy the scalable production of TMD heterostructures, limiting its potential in practical technologies. In order to solve this problem, the current approach is to achieve the direct growth of heterostructures via the CVD method. In terms of the way of stacking, the CVD method not only fabricates vertical heterobilayers or multilayers like mechanical exfoliation but also prepares the in-plane (lateral) heterojunctions. To date, obtaining these two structures by rational design of the synthesis steps and parameters is an important issue in controllable synthesis because of the huge differences in performances of the devices.

4.1. Vertical TMD Heterostructures

2D materials with a dangling-bond-free van der Waals structure break the limitation of the lattice-matching condition of heteroepitaxial growth and thus are promising candidates for vertical heterostructures.[75,76] The growth of TMD-based vertical heterostructures has been intensively developed in the past few years, including TMD/graphene,[77−79] TMD/h-BN,[80,81] TMD/perovskite,[82,83] TMD/iodide,[84,85] TMD/TMD, etc. Among them, TMD/TMD is worthy of great attention, as TMDs with a wide range of band gaps[86] enable heterojunctions with distinct interfaces to be obtained, including metal−metal, semiconductor−semiconductor, and semiconductor−metal, adapting the requirements of diverse electronics and optoelectronics. The growth of the TMD heterostructure is mainly classified into one-step and two-step (or multistep) routes, which were first implemented in 2014[87] and 2015,[88] respectively. One-step growth is more suitable for constructing heterojunctions with two TMDs of similar growth chemistry, including MoS_2−WS_2/WS_2,[89] NbS_2/MoS_2,[90] ReS_2/WS_2,[91] and $MoTe_2/MoS_2$.[92]

Considering the huge differences in the synthesis conditions of the various TMDs, the two-step route is more universal for vertical TMD heterostructures, although its procedures and growth strategies are more complex. The bottom layer should resist high temperatures and complex chemical changes in the second growth process, thus a growth temperature not too high in the second step is crucial to protect the bottom layer. However, the temperature of the second growth process is not as low as possible. Some attempts[93] have been made to change the growth sequence of WS_2 and MoS_2 in a two-step approach,

https://doi.org/10.1021/acsmaterialsau.2c00029
ACS Mater. Au 2022, 2, 665−685

and they found, when following the WS_2−MoS_2 growth sequence, that MoS_2 tended toward in-plane epitaxial growth at the edges of the existing WS_2 triangular single crystal. It was found that while using the MoS_2−WS_2 sequence, WS_2 nucleated from the edge to the crystal center of the MoS_2 triangle to form a vertical bilayer (Figure 5a,b). In the second growth, when MoS_2 is produced under a relatively lower temperature (660 °C), the nucleation rate of MoS_2 on silicon wafers is greater than that on WS_2, so the formation of in-plane heterojunctions is energetically favored. Meanwhile, the second growth temperature is set to a higher growth temperature for WS_2 (800 °C), and the nucleation of MoS_2 is promoted faster, leading to the formation of a rotation misfit-free heterobilayer. In addition to temperature, hydrogen flow is another key factor as well in determining whether a vertical bilayer can be formed, and the absence of hydrogen during the growth process is more conducive to vertical heteroepitaxy[94] in a two-step route.

The two-step route is more versatile and flexible in terms of the product in preparing vertical TMD heterostructures. First, compared to the one-step method, the two-step method avoids cross-contamination and alloying during deposition. Second, the two-step method has realized the tuning of staking modes, providing an optimized platform to study twist-angle-dependent optical physics.[9,95] Third, it also promotes the stacking of TMDs with distinct lattices and phases, implying that metal−semiconductor contact is possible. Several groups have used the two-step approach to obtain a metallic semiconducting vertical heterostructure. A direct synthesis of metallic 1T-VSe_2 onto semiconducting 1H-WSe_2 has been reported and found an inward growth mode of VSe_2 from the edge of WSe_2 to the center (Figure 5c,d).[96] Similar work has been carried out extensively in recent years, including the preparation of VSe_2/$MoSe_2$,[96] NbS_2/WS_2,[97] and ReS_2/MoS_2.[98] According to their band alignments, these heterojunctions either with Schottky or Ohmic contact are valuable for different electronics applications.

In addition to directly depositing TMDs layer by layer with one- or two-step routes, partial substitution is a reliable way to synthesize vertical heterojunctions, as well. In our recent work,[99] Te atoms of crystal 2H-$MoTe_2$ multilayer were replaced inward from the top and bottom layers sequentially, and a sub-centimeter-scale single MoS_2/$MoTe_{2(1-x)}S_{2x}$/MoS_2 sandwich structure was obtained, as presented in Figure 5e,f. This provides an efficient way to obtain large-scale vertical TMD heterostructures with scant grain boundaries.

4.2. Lateral TMD Heterostructures

The lateral TMD heterostructures arouse great scientific interest for their unique atomically sharp interface, where the two sides connect covalently and share one crystal orientation showing a clear and regular boundary without much atomic diffusion.[100−102] Therefore, they are selected candidates in building blocks for diodes and other junction devices utilized in photovoltaics and photodetection.[103,104]

For the preparation of lateral TMD heterostructures, the one-step approach is widely accepted for its high efficiency and controllability. The growth of $MoSe_2$−WSe_2 with lateral heteroepitaxy was reported by physical vapor transport.[101] Later, the preparation of MoS_2−$MoSe_2$ and WS_2−WSe_2 lateral heterostructures via an in situ modulation of the vapor-phase precursors was systematically reported.[105] MoS_2 (WS_2) was synthesized at the first stage to expose peripheral edges where fresh dangling bonds form and serve as the active sites of the following growth of $MoSe_2$ (WSe_2) (Figure 6a). The authors concluded that there are two key factors for the successful synthesis of lateral TMD heterostructures. The first factor is the in situ modulation, which means a rapid switch of the precursor vapor after the first-stage growth and prevents the termination and passivation of edges of TMD formed first. The second factor is optimized growth conditions for both sides of the lateral heterostructures, as already formed 2D TMDs are very sensitive to the changes in the chamber environment. Almost at the same time, MoS_2/WS_2 in-plane heterojunctions were successfully synthesized by the CVD method, as well.[102] It is interesting that they found MoS_2/WS_2 growth can be tuned by adjusting the deposition temperature (Figure 6b). A higher temperature (850 °C) is preferable to obtain a vertical bilayer, while a lower temperature (650 °C) enables the formation of a lateral monolayer. The temperature-selective growth may be explained thermodynamically and kinetically. While ensuring sufficient nucleation and growth rates of both MoS_2 and WS_2, the vertical stacking is more thermodynamically favored, thus it is more stable at a high enough temperature. However, the low temperature significantly prevents the nucleation and growth of WS_2, which causes the epitaxial domain growth from the edge of MoS_2 with less nucleation energy.

The growth of in-plane TMDs heterojunctions is achievable via two-step CVD method, as well. In 2015, in-plane MoS_2−WSe_2 heterojunctions were successfully synthesized via a two-step method.[88] First, the WSe_2 triangle monolayer was deposited at a higher temperature, and it could serve as a seed for the lateral epitaxy growth of MoS_2 at a lower temperature in the second step. This method requires the TMD to grow at a higher temperature as a seed to avoid alloying caused by substitution and decomposition caused by high temperature in the second step. The most typical feature of two-step growth is that it avoids the alloying of the junction at the interface since the growth of inner part and outer part is completed in two different stages separately. Moreover, compared with one-step growth in which similar growth conditions of the two sides are required, it is more universal for controllable in-plane epitaxial growth. It seems that the chronology determines the composition distribution of the heterojunction; that is, the first grown TMD constitutes the core part, and the subsequent in-plane epitaxial growth starts from the edges of the core. However, it has been found that this process is also thermodynamically driven.[106] As illustrated in Figure 6c, the two-step route was used to grow a WS_2 seed and a MoS_2 outer ring, but the product was not WS_2−MoS_2. Instead, the composition distribution was strongly determined by the growth temperature. When the growth temperature was 650 °C, the core was MoS_2 and the ring was $Mo_{1-x}W_xS_2$. When the growth temperature was varied from 680 to 710 °C, core-ring structures disappeared, followed by the formation of a uniformly distributed $Mo_{1-x}W_xS_2$ alloy. This phenomenon can be explained by the interdiffusion of Mo from the edge to the core and W from the core to the edge to reduce its interfacial energy to a minimum, followed by Mo's replacement for W at the core. At higher temperature, the entropic part has a greater effect on the Gibbs free energy, so the products tend to mix more. In contrast, the enthalpic part has more influence on the Gibbs free energy at a relatively lower temperature, and phase segregation is preferable and thus the MoS_2 core surrounded by an alloy ring was synthesized. However, the interdiffusion and alloying could be avoided by system design.

https://doi.org/10.1021/acsmaterialsau.2c00029
ACS Mater. Au 2022, 2, 665−685

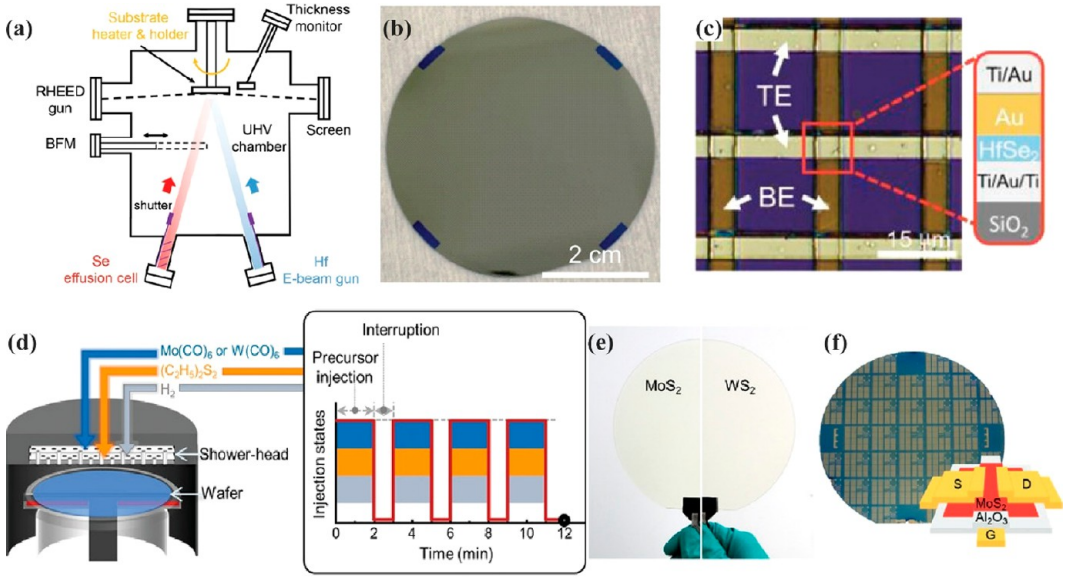

Figure 7. Engineerable fabrication of wafer-scale TMDs and TMD arrays. (a) Schematic of setups and configuration of MBE system for growing wafer-scale $HfSe_2$ thin film. Optical images of (b) MBE-grown $HfSe_2$ on a 2 in. SiO_2/Si substrate and (c) crossbar array as memristors. Reprinted with permission from ref 120. Copyright 2022 Wiley-VCH. (d) Schematic of the MOCVD system with a cyclical supply of gaseous precursors for growing wafer-scale monolayer MoS_2 and WS_2. Optical images of (e) monolayer MoS_2 and WS_2 on 6 in. quart and (f) MoS_2 FET array fabricated by photolithography with Al_2O_3 as the gate dielectric. Reprinted with permission from ref 121. Copyright 2020 Wiley-VCH. Various ways to synthesize wafer-scale TMDs has been explored, and devices fabricated based on these samples are easily arrayed by conventional lithography.

MoS_2−WS_2 and $MoSe_2$−WSe_2 in-plane heterojunctions were also fabricated with 1D interfaces clearly along the zigzag direction using a homemade quartz reactor to separate the Mo vapor and the W vapor.[107]

On this basis, more elaborate in-plane heterojunctions have been synthesized in recent years. The composition-tunable WSe_2−$WS_{2(1-x)}Se_{2x}$ and WS_2−$WS_{2(1-x)}Se_{2x}$ was obtained via a two-step route,[108,109] and such a precise modulation of composition of the heterojunction can be exploited for band alignment engineering. The sequential edge-epitaxy realizing a multijunction lateral heterostructures was reported.[110] Both MoX_2 and WX_2 (X = S or Se) powders were sublimated into oxides and hydroxides at the flow of N_2 and H_2O(g), but the most gaseous W source was hydroxides, thus only the deposition of MoX_2 occurred. When the gas flow was Ar + H_2, the reduction reaction consumed the gaseous Mo oxides, there were relatively more W oxides, and the chemical deposition started due to its low reduction rate.By switching the flow gas back and forth, controllable growth of a striped TMD pattern without complex design was achieved, as shown in Figure 6d−g. WS_2 with WSe_2 nanodots were synthesized by partially damaging the monolayer WS_2 to create growth sites of WSe_2 via O_2 plasma.[111] Moreover, precisely patterning the in-plane TMD heterojunctions is successfully achieved by a lithography-like strategy, which is discussed in detail in the next section.

5. DESIGN AND GROWTH OF TMD-BASED ARRAYS

In order to implement large-scale production of TMD-based heterojunctions and put them into practice, highly ordered TMD arrays need to be realized and integrated. TMD arrays are divided into two types: (1) homogeneous TMD arrays[112] and (2) heterogeneous TMD arrays.[113] To prepare TMD arrays, there are mainly four approaches: (1) patterned etching of wafer-scale 2D TMDs,[74,114] (2) in situ sulfurization/selenization/tellurization,[115] (3) selective sulfurization/selenization,[116] and (4) selective area growth.[117,118]

5.1. Patterned Etching of Wafer-Scale 2D TMDs

The most straightforward method for preparing TMD arrays is to etch wafer-scale 2D TMDs by plasma as required for array patterning.[12,119] The biggest challenge of this route is the preparation of wafer-scale TMDs. In terms of wafer-scale polycrystalline 2D TMD preparation, as shown in Figure 7a−c, molecular beam epitaxy (MBE) was used to thermally combine evaporated Se sources with electron-beam-evaporated Hf sources at a pressure lower than 10^{-8} Torr to prepare 2 in. $HfSe_2$ for arrayed memristors.[120] Compared with MBE, MOCVD does not require a high vacuum. As shown in Figure 7d−f, MOCVD was used with $Mo(CO)_6$ and $(C_2H_5)_2S_2$ as precursors for the preparation of 6 in. monolayer MoS_2 at 5.0 Torr,[121] and an array of MoS_2 devices was obtained, with an average carrier mobility of 3.4 $cm^2\ V^{-1}\ s^{-1}$ by testing the electrical properties of 900 MoS_2 field-effect transistors (FETs). Compared with the MOCVD, LPCVD with a higher reaction temperature for the preparation of TMDs generally obtains high-quality crystals. The 4 in. monolayer MoS_2 films were prepared using precursor multisource distributed vapor deposition, and the monolayers' average room temperature device mobility was ~70 $cm^2\ V^{-1}\ s^{-1}$.[60] The wafer-scale TMDs synthesized above are all polycrystalline materials with more grain boundaries. The grain boundaries of polycrystalline MoS_2 were utilized to fabricate multiterminal memtransistors.[122]

The more grain boundaries there are, the more electron scattering occurs. The small crystal defects and high carrier mobility of single-crystal TMDs make them suitable for a wide range of applications in optoelectronic devices. The controllability of single-crystal 2D TMDs at the wafer-scale plays a pivotal role in moving TMDs toward practical applications. In the preparation of wafer-scale single-crystal 2D TMDs, the phase transition of $MoTe_2$ was used to introduce the crystalline

https://doi.org/10.1021/acsmaterialsau.2c00029
ACS Mater. Au 2022, 2, 665−685

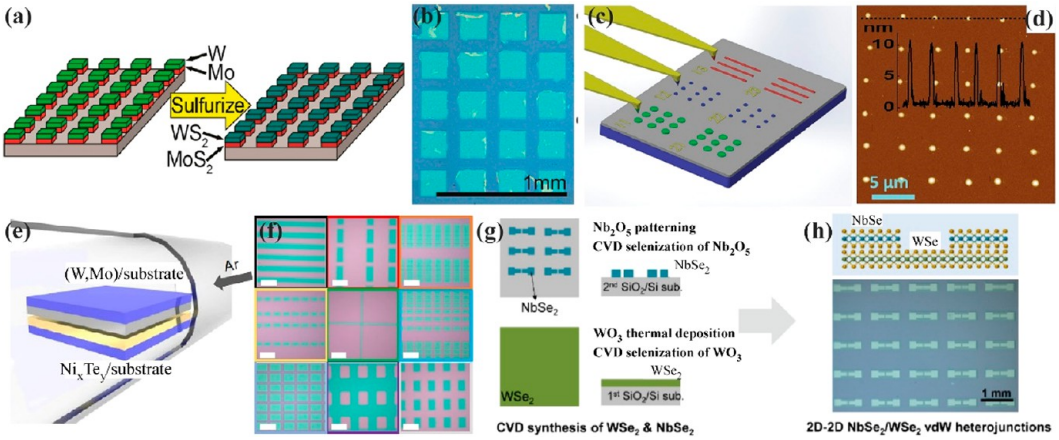

Figure 8. TMD arrays synthesized by in situ sulfurization, selenization, or tellurization. (a) Schematic of patterned W and Mo seeds and their sulfurization to form WS_2/MoS_2 vertical heterojunctions. (b) Optical image of a micron-scale WS_2/MoS_2 vdW heterostructure array. Reprinted from ref 129. Copyright 2016 American Chemical Society. (c) Drawing shows the pattern writing using liquid−metal precursor ink by AFM tips. (d) AFM images of MoS_2 dot arrays with submicron accuracy. Reprinted with permission from ref 130. Copyright 2016 Wiley-VCH. (e) Schematic diagram of the CVD setup to convert W or Mo patterned beforehand by photolithography to WTe_2 or $MoTe_2$ arrays. (f) Optical images of diverse WTe_2 patterns. Scale bar, 100 μm. Reprinted with permission from ref 131. Copyright 2020 Springer Nature. (g) Schematic of Nb_2Se_3 pattern and WSe_2 film through selenization of Nb_2O_3 pattern and WO_3 film. (h) Side view and optical images of $NbSe_2$−WSe_2 patterned heterojunctions. Scale bar, 1 mm. Reprinted from ref 132. Copyright 2017 American Chemical Society. In situ sulfurization/selenization/tellurization is suitable for metal precursors that are easily patterned in a regular way.

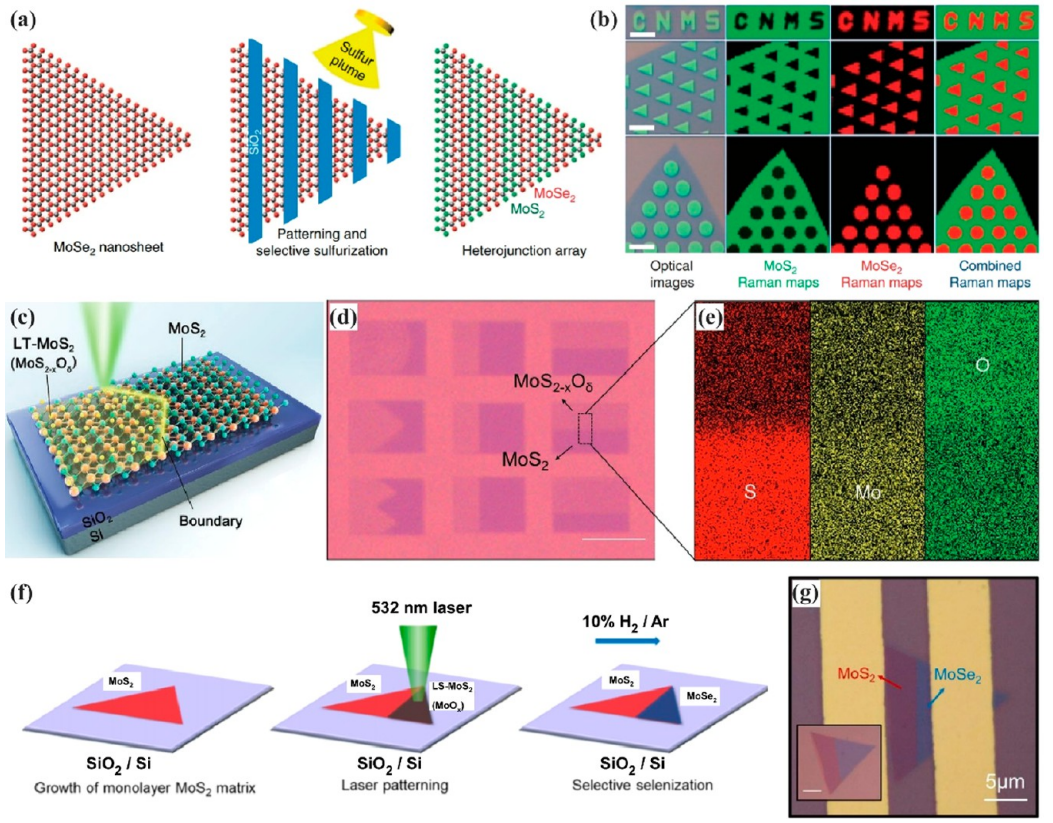

Figure 9. TMD patterns by selective sulfurization. (a) Schematic diagram showing the formation of striped $MoSe_2/MoS_2$ in-plane heterostructures. The SiO_2 mask patterned onto $MoSe_2$ by E-beam lithography protects partial $MoSe_2$ from being converted to MoS_2 by a laser-vaporized sulfur plume. (b) Optical images and Raman mapping of two predefined MoS_2−$MoSe_2$ patterns. Scale bar, 5 μm. Reprinted with permission from ref 134. Copyright 2015 Springer Nature, open access. (c) Schematic view of boundary-editable technology via laser treatment. (d) Optical images of $MoS_2/MoS_{2-x}O_\delta$ later heterojunctions with various types of boundaries. Scale bar, 10 μm. (e) Elemental mapping at the boundary between MoS_2 and $MoS_{2-x}O_\delta$. Reprinted with permission from ref 116. Copyright 2021 Wiley-VCH. (f) Schematic diagram of irradiation-induced selective oxidation of MoS_2 followed by selenization and (g) optical image of junction device based on as-prepared in plane MoS_2−$MoSe_2$. Reprinted from ref 136. Copyright 2021 American Chemical Society. Selective sulfurization finely edits TMDs, enabling the preparation of elaborate in-plane heterojunctions at a small size.

https://doi.org/10.1021/acsmaterialsau.2c00029
ACS Mater. Au 2022, 2, 665−685

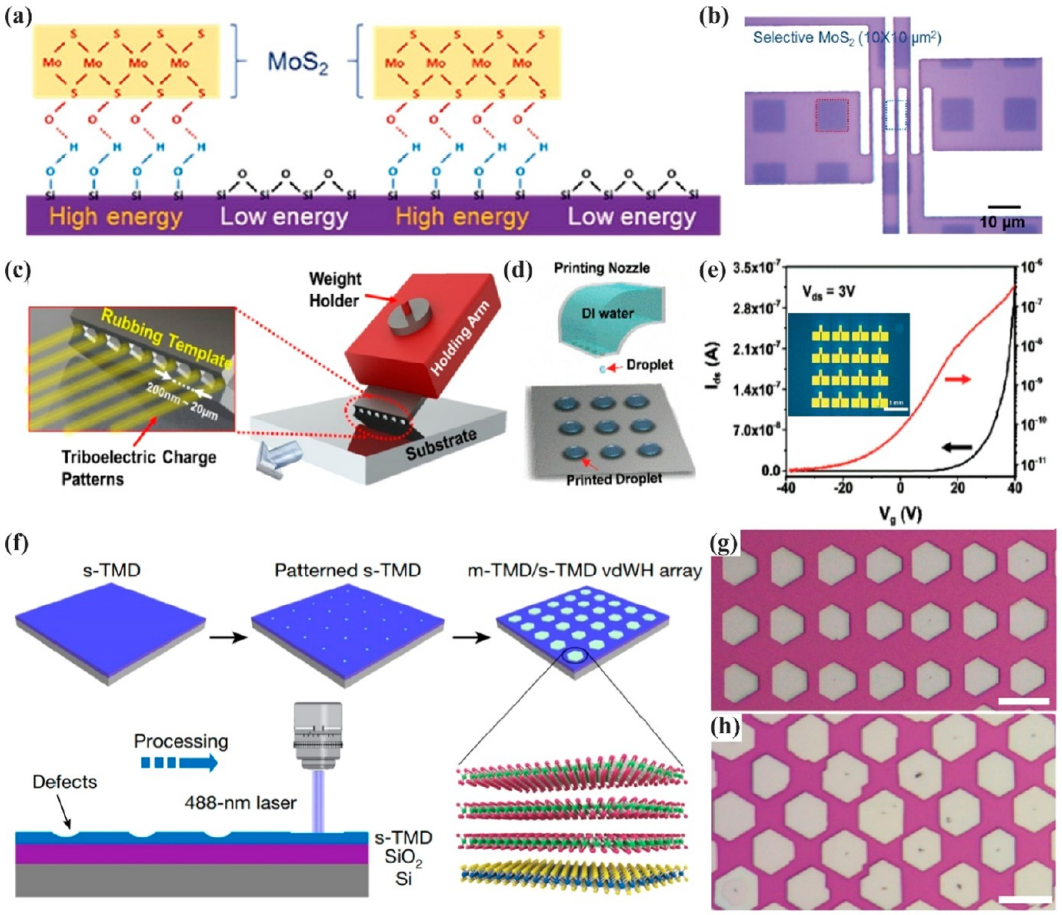

Figure 10. Selective array growth of TMDs arrays via surface treatments. (a) Schematic of selective growth of MoS_2 on energy-differentiated SiO_2/Si surface after O_2 plasma treatment. (b) Optical images of FET fabricated on the MoS_2 array. Reprinted with permission from ref 141. Copyright 2017 Wiley-VCH. (c) Schematic of the formation of triboelectric charge line pattern caused by rubbing, which serves as the nucleation sites for growing MoS_2 in the CVD process. Reprinted from ref 144. Copyright 2018 American Chemical Society. (d) Schematic of inkjet printing of DI water pattern as designated growth sites of MoS_2. (e) Transfer curve of MoS_2-based FET at V_{ds} = 3 V with optical images of FET arrays in the inset. Reprinted with permission from ref 145. Copyright 2020 The Royal Society of Chemistry. (f) Schematic flow of a general way to prepare m-TMD/s-TMD arrays, where irradiation creates defective surfaces to form well-ordered nucleation sites of heteroepitaxy in a two-step CVD method. (g,h) Optical images of VSe_2/WSe_2 vertical heterostructure arrays. Scale bar, 10 μm. Reprinted with permission from ref 146. Copyright 2020 Springer Nature. Diverse treatments can be implemented to create differentiated surfaces for region-selective growth of TMDs.

species 2H-$MoTe_2$ in the center of a wafer-scale 1T′-$MoTe_2$ film to transform metallic 1T′-$MoTe_2$ into wafer-scale single-crystal semiconducting 2H-$MoTe_2$ under a Te atmosphere.[32] The FET arrays, based on 1T′/2H/1T′ $MoTe_2$ obtained from seed-induced phase transition, have effectively reduced contact resistance at the 1T′/2H interface. However, this method is highly limited to TMDs which can easily achieve phase transition.

Array etching of wafer-scale TMDs, which can be achieved directly by a laser beam,[123,124] should minimize the impacts of traditional photolithography glue residue on device performance. Moreover, the high growth temperature destroys the marked substrate, making the transfer of material inevitable before the fabrication of devices. However, the transfer without folding and defects put forward many requirements, such as the use of small molecule polymer transfer[125] or gold film-assisted transfer.[126,127]

5.2. In Situ Sulfurization/Selenization/Tellurization

In situ sulfurization refers to patterning the metal precursor source, followed by sulfurizing the patterned metal precursor.[128] As shown in Figure 8a,b, well-aligned vertical Mo/W layers were deposited by E-beam lithography and sputtering, respectively,[129] and sulfurized into MoS_2/WS_2 vertical heterojunctions. To avoid the phase mixing in the interface, a two-step method was used to in situ sulfide WO_3 and Mo metal precursors sequentially to obtain vertical MoS_2/WS_2 arrays with a photoresponsivity of 2.3 A W^{-1}.[128] It is likely that precursors prepatterned by common mask or lithography possess a poorly defined profile or organic residual adhesive. For this reason, precursor arrays were written with $(NH_4)_2MoS_4$ ink with an atomic force microscopy (AFM) tip on graphene-covered SiO_2/Si substrates[130] and annealed in a CVD chamber with sulfur flow to obtain arrays of MoS_2 (Figure 8c,d). In situ tellurization/selenization is suitable for synthesizing TMDs that are chemically unstable. The patterned W/Mo was used as the metal source with a Ni_xTe_y alloy as the Te source to synthesize patterned WTe_2 on a 4 in. SiO_2/Si substrate, and the Schottky−Mott limit of the metal−semiconductor was achieved (Figure 8e,f).[131] Moreover, as shown in Figure 8g,h, to fabricate $NbSe_2$−WSe_2 metal−semiconductor heterojunction arrays, the Nb_2O_5 pattern and WO_3 thin films were selenized for the formation of $NbSe_2$ arrays and WSe_2 films, respectively.[132]

https://doi.org/10.1021/acsmaterialsau.2c00029
ACS Mater. Au 2022, 2, 665−685

Table 1. Summary of CVD-Grown Large-Scale TMDs

materials	architectures[a]	methods	characteristics	applications	ref
MoS_2	ML	APCVD	wafer-scale thin film	flexible FETs	164
	ML	LPCVD	wafer-scale thin film	FETs, logic inverters	60
	ML	APCVD	centimeter-scale thin film, single crystallinity	FETs	47
	ML	LPCVD	wafer-scale thin film, single crystallinity	FET array	55
	multilayer	MOCVD	thin film on glass	low-power photodetectors	170
	ML	MOCVD	wafer-scale thin film		66
	ML	MOCVD	centimeter-scale thin film	FETs	68
MoS_2 or $MoSe_2$	ML	APCVD	millimeter-scale single crystals	FETs	48
WS_2	ML	MOCVD	wafer-scale thin film, single crystallinity	FETs	69
	ML	LPCVD	wafer-scale thin film, single crystallinity		54
WSe_2	ML or BL	APCVD	millimeter-scale single crystals	FETs	166
$MoSe_2$	ML	APCVD	centimeter-scale thin film,		49
$MoTe_2$	multilayer	APCVD	centimeter-scale single crystals	FETs	32,99,167

[a]ML, monolayer; BL, bilayer.

5.3. Selective Sulfurization/Selenization

Selective sulfurization is essentially the localized substitution of chalcogen atoms of TMDs in the atmosphere of the desired gas.[133] Mimicking the lithography process, TMDs are masked with an inert material pattern and converted to other TMDs in a specific gas flow, thus an artificially designed pattern is realized. As present in Figure 9a,b, striped SiO_2 was deposited as a mask on the $MoSe_2$ nanosheet, and the sulfur source was evaporated to transform exposed $MoSe_2$ to MoS_2 at 700 °C, constructing the $MoSe_2$−MoS_2 lateral array with a type I alignment.[134] Such a method involves a covered layer, inevitably introducing impurities that affect the performance of the device, so a high energy laser is used to achieve selective conversion of the TMD. Laser-assisted selective conversion of $MoSe_2$ to MoS_2 in H_2S/H_2 mixed gas was completed,[135] suggesting that the laser is able to provide a new platform to extend the controllability of TMD array growth. Figure 9c−e demonstrates the preparation of $MoS_2/MoS_{2-x}O_\delta$ heterojunctions by creating multiple S vacancies on MoS_2 and slightly oxidizing it to $MoS_{2-x}O_\delta$ by high-energy laser treatment.[116] The $MoS_2/MoS_{2-x}O_\delta$ heterojunction was used to fabricate synaptic devices, which exhibited both short- and long-term plasticity in response to electricity and light-based stimulation simultaneously. On this basis, as presented in Figure 9f,g, the pattern on MoS_2 was directly written and oxidized to MoO_X, followed by the selenization to $MoSe_2$ to form the $MoSe_2/MoS_2$ in-plane heterostructure,[136] implying that a nanoscale precise patterning is available.

5.4. Selective Area Array Growth

Selective area growth is mainly achieved by surface treatment of the growth substrate[137] to create differentiated local growth environment for TMDs[138−140] to selectively grow TMD arrays directly. As demonstrated in Figure 10a,b, SiO_2/Si substrates were treated with oxygen plasma to enhance the surface energy, followed by the preparation of MoS_2 using the CVD method, where MoS_2 would selectively grow in the arrayed regions with high surface energy, and polycrystalline MoS_2 arrays were achieved.[141] The oxygen plasma was used to etch SiO_2/Si substrates partially covered with graphene to enhance the hydrophilicity of the SiO_2 surface so that MoS_2 was selectively grown on the plasma-treated SiO_2 surface, and MoS_2-graphene lateral heterojunction arrays were obtained consequently.[142] Based on this, graphene could serve as source-drain electrodes of the FET, and the measured carrier mobility was about 17 $cm^2\ V^{-1}\ s^{-1}$. This method is universal for the preparation of TMD-based lateral interfacial heterojunctions. Moreover, surfactant-mediated concept of using Na ions as surfactants was proposed to prepare monolayer TMD materials.[143] The 6 × 6 arrays of NaBr were deposited on a 4 × 1 cm^{-2} SiO_2/Si substrate, and subsequently MoS_2 would selectively grow in the NaBr region to realize patterning of MoS_2. As shown in Figure 10c, a rubbing tool was utilized to introduce triboelectric charge of the surface of SiO_2/Si substrate, and MoS_2 would selectively grow on the areas with frictional charges to produce arrayed MoS_2 in CVD growth.[144] The arrays, with an average carrier mobility of 0.18 ± 0.17 $cm^2\ V^{-1}\ s^{-1}$ and high switching ratio of ∼8, could be cost-efficient for MoS_2 memristors.

Through preparation of nucleation sites for arrays, Figure 10d,e illustrates the inkjet printing technique[145] to define an array of microscale deionized (DI) water droplets on substrates, leaving arrays of water traces when the water evaporates. Then MoS_2 will selectively grow on the array's water traces and FETs based on the array was tested with a carrier mobility of approximately 0.15 $cm^2V^{-1}s^{-1}$. The ink printing technique greatly improves the efficiency of preparation of array precursor, but the crystal quality of MoS_2 needs to be further improved. In 2020, a general approach was proposed to prepare a series TMD arrays grown on WSe_2 including VSe_2 (Figure 10f−h),[146] $NiTe_2$, $CoTe_2$, $NbTe_2$, and VS_2. The matrix of defect spots was created on s-TMD by laser beam to form nucleation sites for the second TMD. The nucleation sites etched by laser avoid the influence of photolithographic glue residue, and high-quality TMD single crystals were prepared directly by CVD to obtain arrays of TMD heterojunctions.

6. APPLICATIONS OF CVD-GROWN TMDs

2D TMDs are particularly attractive in the field of micro/nanoelectronics due to their superior mechanical, transport, and optoelectronic properties. For mechanical properties, the 2D nature overcomes the shortcomings of rigidness and brittleness, making 2D TMDs outstanding candidates for flexible electronics including FETs,[147] supercapacitors,[148] logic gates, and oscillators.[149] In terms of transport performance, theoretical mobility of TMDs ranges from 10 to 1000 $cm^2\ V^{-1}\ s^{-1}$, an impressive upper limit.[150] 2D TMDs are especially competitive in optoelectronics among low-dimensional materials for several reasons: (1) 2D TMDs realize photoresponse to

https://doi.org/10.1021/acsmaterialsau.2c00029
ACS Mater. Au 2022, 2, 665−685

Table 2. Summary of CVD-Grown TMD Heterostructures

materials	architectures[a]	methods (step)	characteristics	applications	ref
MoS_2/WS_2	LHS or VHS	APCVD (1)	clean interface	FETs	102,171
	LHS or VHS	LPCVD (2)	clean interface		93,94
	LHS	APCVD (1)	photovoltaic effect	self-powered photodetector	90
$MoSe_2/WSe_2$	LHS	LPCVD (1)	p−n junction photovoltaic effect	photodetectors, light emitting diodes	168
	VHS	APCVD (2)	p−n junction, strongly coupled vdW heterostructures	excitonic devices	88,172
WSe_2/MoS_2	LHS	LPCVD (2)	p−n junction photovoltaic effect	photodetectors	88
WSe_2/WS_2	LHS	APCVD (2)	WSe_2 puddle in WS_2	photogating photodetectors	111
$WSe_2/WS_{2(1-x)}Se_2$	VHS	APCVD (2)	strongly coupled vdW heterostructures		96
$WS_2/WS_{2(1-x)}Se_2$	VHS	APCVD (2)			97
MS_2-MSe_2 (M= Mo, W)	LHS	APCVD (2)	clean interface	FETs, complementary metal−oxide semiconductor	105
MoX_2-WX_2 (X= S, Se)	LHS	APCVD (1)	clean interface		107
	VHS	APCVD (2)	strongly coupled vdW heterostructures		95,173
MoS_2−WS_2/WS_2	LHS and VHS	APCVD (1)	LHS and VHS achieved in one structure		89
VS_2/WS_2	LHS	APCVD (2)	1T-2H metal−semiconductor contact	FETs	169
VSe_2/MX_2 (M = Mo, W; X = S, Se)	VHS	APCVD (2)	1T-1H metal−semiconductor contact		96
$MoTe_2/MoS_2$	VHS	APCVD (2)	p−n junction	UV−vis−IR photodetectors	92
$MoTe_2/MoTe_2$	LHS	APCVD (2)	1T′-2H-1T′ metal−semiconductor−metal contact	FET array	32
MTe_2 (M = V, Nb, Ta)/ WSe_2 (WS_2)	VHS	APCVD (2)	1T-2H metal−semiconductor contact	FETs	174
$CrSe_2/WSe_2$	VHS	APCVD (2)	thickness-dependent magnetic order	Hall devices	175
NbS_2/MoS_2	VHS	APCVD (1)	R-type stacking metal−semiconductor contact		90
NbS_2/WS_2	VHS	APCVD (2)	1T-1H metal−semiconductor contact		97
ReS_2/WS_2	VHS	APCVD (1)	fully covered twinned bilayer		91
ReS_2/MoS_2	LHS	APCVD (2)	2H-1T′ type I band alignment		98
$MoS_2/MoTe_{2(1-x)}S_{2x}/MoS_2$	VHS	APCVD (2)	centimeter-scale heterostructure		99

[a]VHS, vertical heterostructure; LHS, lateral vertical heterostructure.

Table 3. Summary of CVD-Patterned TMDs

materials	architectures	methods	applications	ref
MoS_2	array	selective-area growth	FET array	145
	array	selective-area growth	FETs	141
	patten	selective sulfurization	FETs, memristors	144
	array	patterned etching	FET array	122
MoS_2 or WS_2	array	patterned etching	FET array	121
MoS_2/WS_2	array	in situ sulfurization	transistor, hydrogen evolution reaction catalysts	128,129
$NbSe_2$−WSe_2	array	in situ selenization	FETs	132
MoS_2−$MoSe_2$	patten	selective sulfurization/selenization	FETs	134,136
WTe_2 or $MoTe_2$	array	in situ tellurization	FETs	131
$MoS_2/MoS_{2-x}O_\delta$	patten	selective sulfurization	synaptic devices	116
VSe_2 ($NiTe_2$, $CoTe_2$, $NbTe_2$,VS_2)/WSe_2	array	selective sulfurization	FET array	146

https://doi.org/10.1021/acsmaterialsau.2c00029
ACS Mater. Au 2022, 2, 665−685

a broad spectrum. On one hand, due to the wide variety of TMDs, wavelengths from visible to near-infrared can be realized.[151] On the other hand, methods such as modulation by alloying[152,153] and external force[154−158] are highly applicable to 2D TMDs, enabling the artificial band gap with tunability. Moreover, the photodetection range of TMDs can be efficiently expanded by means of heterojunctions. The recently reported interlayer excitons detected in various TMD heterostructures have revealed great potential of TMDs for long-wavelength infrared photodetection.[159,160] (2) A considerable part of the 2D TMDs is materials with strong light−matter coupling.[161,162] When the TMD film is a monolayer, there is a conversion from an indirect band gap to a direct band gap for TMD materials, such as MoS_2, WSe_2, or $MoTe_2$. (3) 2D TMDs enable an ultrafast photodetection with response times of low to hundreds of nanoseconds.[19,163] In addition, the strong spin−orbit coupling and broken inversion symmetry of TMDs reveal non-negligible potential for applications in spintronics and valleytronics.[53] To illustrate the application scenarios of 2D TMDs more concretely, Tables 1−3 summarize TMD materials included in this review and their representative electronics reported.

Table 1 focuses on examples of large-scale highly crystalline semiconducting TMDs, which shows great potential for monolithic integration of chips. For the fabrication of TMD-based electronics, one of the most pressing tasks is to realize the synthesis of boundary-free wafer-scale TMDs with uniform and low thickness. In fact, it is not difficult to meet any of these requirements individually, but the key is to satisfy them simultaneously. It is noted that recent progress has been made in preparing single-crystal wafer-scale monolayer MS_2 (M = Mo, W),[47,54,55,69] while no other TMD with such features has been synthesized successfully. These wafer-scale TMDs with high quality are used as semiconductor channels in FETs and FET arrays on the whole. Moreover, large-scale integrated arrays can be transferred onto flexible polymer substrates to form flexible FET devices.[164] It is believed that, in the next few years, similar work and applications based on other TMD materials will significantly increase, as millimeter-scale monolayer single crystals such as $MoSe_2$[165] and WSe_2[166] have been successfully obtained. Specifically, wafer-scale multilayer $MoTe_2$ with centimeter-scale single-crystal domains can be synthesized by phase transition.[32,99,167]

Table 2 lists CVD-grown TMD heterostructures, in which it is found that one-step or one-pot methods are preferable for the synthesis of lateral heterojunctions, whereas the two-step route satisfies the demands of preparation of both lateral and vertical heterostructures. Devices based on bare TMDs are extremely limited in both functionality and performance. For instance, there is no effect rectification found in devices made of pure individually CVD-grown monolayer $MoSe_2$ or WSe_2, but the in-plane $MoSe_2$−WSe_2 heterostructure exhibits I−V characteristics of a typical p−n junction and can be applied as both self-powered photodetectors and electroluminescent photon emitters.[168] Moreover, a heterostructure composed of two types of TMDs is commonly a type II band alignment, which is highly efficient to separate photoexcited electrons and holes and suitable for photodetectors.[163] In addition to being used as active channels, TMDs can act as metal electrodes, as well. For example, in the lateral VS_2−MoS_2 heterostructure, the metallic VS_2 serves as the contact between the Ni/Au electrode and MoS_2, decreasing the Schottky barrier to ∼30 meV.[169]

Table 3 shows TMD-based arrays and patterns obtained via the four approaches mentioned. Patterned etching relies on proven synthesis technology for large-scale TMDs, thus it is mostly used in the fabrication of well-aligned active channels on wafers.[121,122] To achieve more complex and wide-ranging application scenarios, heterostructures with a wafer size as well as a well-defined boundary are required as discussed above, which is expected to be achieved by in situ sulfurization/selenization/tellurization,[128,129,131,132] selective sulfurization/selenization,[116,134,144,146] and selective area growth.[141,145]

7. PERSPECTIVES FOR CVD GROWTH OF TMDs

In general, CVD is currently one of most promising approaches to meet the practical demand for production of 2D TMDs, due to its ability to produce large-area thin film and high controllability. The related research concentrates on the synthesis of wafer-scale and boundary-free TMD thin films, TMD heterostructures with designed architectures, and pattered TMD arrays. Although the recent decade has seen a boom in engineering of TMDs and TMD heterostructures, there remains a lot of tough problems to be solved. The primary issue is the scarcity of a general method to mass produce wafer-scale single-crystal TMDs, with limited varieties and substrates failing to satisfy the demands in various applications. To date, the success made in the synthesis of high-quality wafer-scale TMDs mainly comes from common species like MoS_2 and WS_2, and the research on most other TMDs has not progressed. Although highly oriented TMD domains could be achieved by the selection of growth substrates, few of these substrates support a transfer-free route to fabricate electronics, and it may bring transfer-induced imperfections including defects, wrinkles, folds, impurities, and bubbles.

Moreover, further improvement of controllability of the CVD process is urgently required, as well. Although many studies in recent years have emphasized that defects can be effectively improved, defects are a prominent shortcoming of CVD-grown materials which are not competitive with those exfoliated equivalents. Further thermodynamic and kinetic studies related to CVD growth mechanisms need to be developed to assist the refinement of CVD-grown crystal structures. In addition, further improvement of controllability is urgently required, as well. Twist angle, as one of the hottest trending topics in the field of 2D materials due to unconventional physical phenomena originating from it, is extensively studied using artificially stacked TMDs. However, the transfer process inevitably destroys the interlayer interface, and the size of such samples is usually less than 100 μm, resulting in deviations in related measurements. Therefore, a twist-angle-tunable synthesis approach of bilayer or multilayer TMDs is pursued. Moreover, the poor reproducibility of experiments is still a great challenge, and this undoubtedly impedes their further commercialization. Thus, how to create a stable local growth environment under vapor flow by improving equipment setup is a key consideration in future work.

AUTHOR INFORMATION

Corresponding Author

Zhengtang Luo − *Department of Chemical and Biological Engineering, Guangdong-Hong Kong-Macao Joint Laboratory for Intelligent Micro-Nano Optoelectronic Technology,*

https://doi.org/10.1021/acsmaterialsau.2c00029
ACS Mater. Au 2022, 2, 665−685

William Mong Institute of Nano Science and Technology, and Hong Kong Branch of Chinese National Engineering Research Center for Tissue Restoration and Reconstruction, Hong Kong University of Science and Technology, Kowloon 999077, Hong Kong, P.R. China; orcid.org/0000-0002-5134-9240; Email: keztluo@ust.hk

Authors

Ting Kang − *Department of Chemical and Biological Engineering, Guangdong-Hong Kong-Macao Joint Laboratory for Intelligent Micro-Nano Optoelectronic Technology, William Mong Institute of Nano Science and Technology, and Hong Kong Branch of Chinese National Engineering Research Center for Tissue Restoration and Reconstruction, Hong Kong University of Science and Technology, Kowloon 999077, Hong Kong, P.R. China*

Tsz Wing Tang − *Department of Chemical and Biological Engineering, Guangdong-Hong Kong-Macao Joint Laboratory for Intelligent Micro-Nano Optoelectronic Technology, William Mong Institute of Nano Science and Technology, and Hong Kong Branch of Chinese National Engineering Research Center for Tissue Restoration and Reconstruction, Hong Kong University of Science and Technology, Kowloon 999077, Hong Kong, P.R. China*

Baojun Pan − *Macao Institute of Materials Science and Engineering (MIMSE), Macau University of Science and Technology, Taipa, Macau 999078, P.R. China*

Hongwei Liu − *Department of Chemical and Biological Engineering, Guangdong-Hong Kong-Macao Joint Laboratory for Intelligent Micro-Nano Optoelectronic Technology, William Mong Institute of Nano Science and Technology, and Hong Kong Branch of Chinese National Engineering Research Center for Tissue Restoration and Reconstruction, Hong Kong University of Science and Technology, Kowloon 999077, Hong Kong, P.R. China;* orcid.org/0000-0001-7566-5224

Kenan Zhang − *Department of Chemical and Biological Engineering, Guangdong-Hong Kong-Macao Joint Laboratory for Intelligent Micro-Nano Optoelectronic Technology, William Mong Institute of Nano Science and Technology, and Hong Kong Branch of Chinese National Engineering Research Center for Tissue Restoration and Reconstruction, Hong Kong University of Science and Technology, Kowloon 999077, Hong Kong, P.R. China*

Complete contact information is available at: https://pubs.acs.org/10.1021/acsmaterialsau.2c00029

Author Contributions

[§]T.K., T.W.T., and B.P. contributed equally.

Notes

The authors declare no competing financial interest.

ACKNOWLEDGMENTS

Z.L. acknowledge supports by the RGC (16304421), the Innovation and Technology Commission (ITC-CNERC14SC01), Guangdong Science and Technology Department (Project# 2020A0505090003), Research Fund of Guangdong-Hong Kong-Macao Joint Laboratory for Intelligent Micro-Nano Optoelectronic Technology (No. 2020B1212030010), the IER Foundation (HT-JD-CXY-201907), "International science and technology cooperation projects" of Science and Technological Bureau of Guangzhou Huangpu District (2019GH06), and Shenzhen Special Fund for Central Guiding the Local Science and Technology Development (2021Szvup136).

REFERENCES

(1) Cao, Y.; Fatemi, V.; Fang, S.; Watanabe, K.; Taniguchi, T.; Kaxiras, E.; Jarillo-Herrero, P. Unconventional superconductivity in magic-angle graphene superlattices. *Nature* **2018**, *556* (7699), 43−50.

(2) Yoo, H.; Engelke, R.; Carr, S.; Fang, S.; Zhang, K.; Cazeaux, P.; Sung, S. H.; Hovden, R.; Tsen, A. W.; Taniguchi, T.; Watanabe, K.; Yi, G. C.; Kim, M.; Luskin, M.; Tadmor, E. B.; Kaxiras, E.; Kim, P. Atomic and electronic reconstruction at the van der Waals interface in twisted bilayer graphene. *Nat. Mater.* **2019**, *18* (5), 448−453.

(3) Liu, H.; Mendelson, N.; Abidi, I. H.; Li, S.; Liu, Z.; Cai, Y.; Zhang, K.; You, J.; Tamtaji, M.; Wong, H.; Ding, Y.; Chen, G.; Aharonovich, I.; Luo, Z. Rational control on quantum emitter formation in carbon-doped monolayer hexagonal boron nitride. *ACS Appl. Mater. Interfaces* **2022**, *14* (2), 3189−3198.

(4) Liu, H.; You, C. Y.; Li, J.; Galligan, P. R.; You, J.; Liu, Z.; Cai, Y.; Luo, Z. Synthesis of hexagonal boron nitrides by chemical vapor deposition and their use as single photon emitters. *Nano Mater. Sci.* **2021**, *3* (3), 291−312.

(5) Liu, L.; Kong, L.; Li, Q.; He, C.; Ren, L.; Tao, Q.; Yang, X.; Lin, J.; Zhao, B.; Li, Z.; Chen, Y.; Li, W.; Song, W.; Lu, Z.; Li, G.; Li, S.; Duan, X.; Pan, A.; Liao, L.; Liu, Y. Transferred van der Waals metal electrodes for sub-1-nm MoS_2 vertical transistors. *Nat. Electron.* **2021**, *4* (5), 342−347.

(6) Liu, Y.; Weiss, N. O.; Duan, X.; Cheng, H.-C.; Huang, Y.; Duan, X. Van der Waals heterostructures and devices. *Nat. Rev. Mater.* **2016**, *1* (9), 16042.

(7) Wu, Z.; Zhou, B. T.; Cai, X.; Cheung, P.; Liu, G. B.; Huang, M.; Lin, J.; Han, T.; An, L.; Wang, Y.; Xu, S.; Long, G.; Cheng, C.; Law, K. T.; Zhang, F.; Wang, N. Intrinsic valley Hall transport in atomically thin MoS_2. *Nat. Commun.* **2019**, *10* (1), 611.

(8) Cai, X.; An, L.; Feng, X.; Wang, S.; Zhou, Z.; Chen, Y.; Cai, Y.; Cheng, C.; Pan, X.; Wang, N. Layer-dependent interface reconstruction and strain modulation in twisted WSe_2. *Nanoscale* **2021**, *13* (32), 13624−13630.

(9) Yuan, L.; Zheng, B.; Kunstmann, J.; Brumme, T.; Kuc, A. B.; Ma, C.; Deng, S.; Blach, D.; Pan, A.; Huang, L. Twist-angle-dependent interlayer exciton diffusion in WS_2−WSe_2 heterobilayers. *Nat. Mater.* **2020**, *19* (6), 617−623.

(10) Wang, Z.; Rhodes, D. A.; Watanabe, K.; Taniguchi, T.; Hone, J. C.; Shan, J.; Mak, K. F. Evidence of high-temperature exciton condensation in two-dimensional atomic double layers. *Nature* **2019**, *574* (7776), 76−80.

(11) Wang, L.; Wu, Y.; Yu, Y.; Chen, A.; Li, H.; Ren, W.; Lu, S.; Ding, S.; Yang, H.; Xue, Q. K.; Li, F. S.; Wang, G. Direct observation of one-dimensional Peierls-type charge density wave in twin boundaries of monolayer $MoTe_2$. *ACS Nano* **2020**, *14* (7), 8299−8306.

(12) Xu, H.; Zhang, H.; Guo, Z.; Shan, Y.; Wu, S.; Wang, J.; Hu, W.; Liu, H.; Sun, Z.; Luo, C.; Wu, X.; Xu, Z.; Zhang, D. W.; Bao, W.; Zhou, P. High-performance wafer-scale MoS_2 transistors toward practical application. *Small* **2018**, *14* (48), No. 1803465.

(13) Yu, L.; El-Damak, D.; Radhakrishna, U.; Ling, X.; Zubair, A.; Lin, Y.; Zhang, Y.; Chuang, M. H.; Lee, Y. H.; Antoniadis, D.; Kong, J.; Chandrakasan, A.; Palacios, T. Design, modeling, and fabrication of chemical vapor deposition grown MoS_2 circuits with E-mode FETs for large-area electronics. *Nano Lett.* **2016**, *16* (10), 6349−6356.

(14) Kim, Y.; Lee, S.; Song, J. G.; Ko, K. Y.; Woo, W. J.; Lee, S. W.; Park, M.; Lee, H.; Lee, Z.; Choi, H.; Kim, W. H.; Park, J.; Kim, H. 2D transition metal dichalcogenide heterostructures for p-and n-type photovoltaic self-powered gas sensor. *Adv. Funct. Mater.* **2020**, *30* (43), 2003360.

(15) Bonilla, M.; Kolekar, S.; Ma, Y.; Diaz, H. C.; Kalappattil, V.; Das, R.; Eggers, T.; Gutierrez, H. R.; Phan, M.-H.; Batzill, M. Strong

room-temperature ferromagnetism in VSe_2 monolayers on van der Waals substrates. *Nat. Nanotechnol.* **2018**, *13* (4), 289−293.
(16) Fu, S.; Kang, K.; Shayan, K.; Yoshimura, A.; Dadras, S.; Wang, X.; Zhang, L.; Chen, S.; Liu, N.; Jindal, A.; Li, X.; Pasupathy, A. N.; Vamivakas, A. N.; Meunier, V.; Strauf, S.; Yang, E. H. Enabling room temperature ferromagnetism in monolayer MoS_2 via in situ iron-doping. *Nat. Commun.* **2020**, *11* (1), 2034.
(17) Weston, A.; Castanon, E. G.; Enaldiev, V.; Ferreira, F.; Bhattacharjee, S.; Xu, S.; Corte-Leon, H.; Wu, Z.; Clark, N.; Summerfield, A.; Hashimoto, T.; Gao, Y.; Wang, W.; Hamer, M.; Read, H.; Fumagalli, L.; Kretinin, A. V.; Haigh, S. J.; Kazakova, O.; Geim, A. K.; Fal'ko, V. I.; Gorbachev, R. Interfacial ferroelectricity in marginally twisted 2D semiconductors. *Nat. Nanotechnol.* **2022**, *17* (4), 390−395.
(18) Wu, D.; Guo, J.; Wang, C.; Ren, X.; Chen, Y.; Lin, P.; Zeng, L.; Shi, Z.; Li, X. J.; Shan, C. X.; Jie, J. Ultrabroadband and high-detectivity photodetector based on WS_2/Ge heterojunction through defect engineering and interface passivation. *ACS Nano* **2021**, *15* (6), 10119−10129.
(19) Zhang, Y.; Ma, K.; Zhao, C.; Hong, W.; Nie, C.; Qiu, Z.-J.; Wang, S. An ultrafast WSe_2 photodiode based on a lateral pin homojunction. *ACS Nano* **2021**, *15* (3), 4405−4415.
(20) Zhuang, M.; Xu, G.-L.; Gan, L.-Y.; Dou, Y.; Sun, C.-J.; Ou, X.; Xie, Y.; Liu, Z.; Cai, Y.; Ding, Y.; Abidi, I. H.; Tyagi, A.; Amine, K.; Luo, Z. Sub-5 nm edge-rich 1T′-$ReSe_2$ as bifunctional materials for hydrogen evolution and sodium-ion storage. *Nano Energy* **2019**, *58*, 660−668.
(21) Liu, Y.; Su, Y.; Guan, J.; Cao, J.; Zhang, R.; He, M.; Gao, K.; Zhou, L.; Jiang, Z. 2D heterostructure membranes with sunlight-driven self-cleaning ability for highly efficient oil−water separation. *Adv. Funct. Mater.* **2018**, *28* (13), 1706545.
(22) Ko, C.; Lee, Y.; Chen, Y.; Suh, J.; Fu, D.; Suslu, A.; Lee, S.; Clarkson, J. D.; Choe, H. S.; Tongay, S.; Ramesh, R.; Wu, J. Ferroelectrically gated atomically thin transition-metal dichalcogenides as nonvolatile memory. *Adv. Mater.* **2016**, *28* (15), 2923−30.
(23) Li, H.; Lu, G.; Wang, Y.; Yin, Z.; Cong, C.; He, Q.; Wang, L.; Ding, F.; Yu, T.; Zhang, H. Mechanical exfoliation and characterization of single-and few-layer nanosheets of WSe_2, TaS_2, and $TaSe_2$. *Small* **2013**, *9* (11), 1974−1981.
(24) Hai, X.; Chang, K.; Pang, H.; Li, M.; Li, P.; Liu, H.; Shi, L.; Ye, J. Engineering the edges of MoS_2 (WS_2) crystals for direct exfoliation into monolayers in polar micromolecular solvents. *J. Am. Chem. Soc.* **2016**, *138* (45), 14962−14969.
(25) Fan, X.; Xu, P.; Li, Y. C.; Zhou, D.; Sun, Y.; Nguyen, M. A. T.; Terrones, M.; Mallouk, T. E. Controlled exfoliation of MoS_2 crystals into trilayer nanosheets. *J. Am. Chem. Soc.* **2016**, *138* (15), 5143−5149.
(26) Ohring, M.; Zarrabian, S.; Grogan, A. The materials science of thin films. *Appl. Opt.* **1992**, *31* (34), 7162.
(27) Xu, M.; Tang, B.; Lu, Y.; Zhu, C.; Lu, Q.; Zhu, C.; Zheng, L.; Zhang, J.; Han, N.; Fang, W.; Guo, Y.; Di, J.; Song, P.; He, Y.; Kang, L.; Zhang, Z.; Zhao, W.; Guan, C.; Wang, X.; Liu, Z. Machine learning driven synthesis of few-layered WTe_2 with geometrical control. *J. Am. Chem. Soc.* **2021**, *143* (43), 18103−18113.
(28) Gan, L.; Luo, Z. Turning off hydrogen to realize seeded growth of subcentimeter single-crystal graphene grains on copper. *ACS Nano* **2013**, *7* (10), 9480−9488.
(29) Tang, B.; Lu, Y.; Zhou, J.; Chouhan, T.; Wang, H.; Golani, P.; Xu, M.; Xu, Q.; Guan, C.; Liu, Z. Machine learning-guided synthesis of advanced inorganic materials. *Mater. Today* **2020**, *41*, 72−80.
(30) Wang, R.; Yu, Y.; Zhou, S.; Li, H.; Wong, H.; Luo, Z.; Gan, L.; Zhai, T. Strategies on phase control in transition metal dichalcogenides. *Adv. Funct. Mater.* **2018**, *28* (47), 1802473.
(31) Luxa, J.; Spejchalová, L.; Jakubec, I.; Sofer, Z. MoS_2 stacking matters: 3R polytype significantly outperforms 2H MoS_2 for the hydrogen evolution reaction. *Nanoscale* **2021**, *13* (46), 19391−19398.
(32) Xu, X.; Pan, Y.; Liu, S.; Han, B.; Gu, P.; Li, S.; Xu, W.; Peng, Y.; Han, Z.; Chen, J.; Gao, P.; Ye, Y. Seeded 2D epitaxy of large-area single-crystal films of the van der Waals semiconductor 2H $MoTe_2$. *Science* **2021**, *372* (6538), 195−200.
(33) Chhowalla, M.; Shin, H. S.; Eda, G.; Li, L.-J.; Loh, K. P.; Zhang, H. The chemistry of two-dimensional layered transition metal dichalcogenide nanosheets. *Nat. Chem.* **2013**, *5* (4), 263−275.
(34) Leng, K.; Chen, Z.; Zhao, X.; Tang, W.; Tian, B.; Nai, C. T.; Zhou, W.; Loh, K. P. Phase restructuring in transition metal dichalcogenides for highly stable energy storage. *ACS Nano* **2016**, *10* (10), 9208−9215.
(35) Wang, Z.; Shen, Y.; Ito, Y.; Zhang, Y.; Du, J.; Fujita, T.; Hirata, A.; Tang, Z.; Chen, M. Synthesizing 1T-1H two-phase $M_{1-x}W_xS_2$ monolayers by chemical vapor deposition. *ACS Nano* **2018**, *12* (2), 1571−1579.
(36) Yin, H.; Zhang, X.; Lu, J.; Geng, X.; Wan, Y.; Wu, M.; Yang, P. Substrate effects on the CVD growth of MoS_2 and WS_2. *J. Mater. Sci.* **2020**, *55* (3), 990−996.
(37) Zhang, Y.; Yao, Y.; Sendeku, M. G.; Yin, L.; Zhan, X.; Wang, F.; Wang, Z.; He, J. Recent progress in CVD growth of 2D transition metal dichalcogenides and related heterostructures. *Adv. Mater.* **2019**, *31* (41), 1901694.
(38) Thangaraja, A.; Shinde, S. M.; Kalita, G.; Tanemura, M. Effect of WO_3 precursor and sulfurization process on WS_2 crystals growth by atmospheric pressure CVD. *Mater. Lett.* **2015**, *156*, 156−160.
(39) Ling, X.; Lee, Y.-H.; Lin, Y.; Fang, W.; Yu, L.; Dresselhaus, M. S.; Kong, J. Role of the seeding promoter in MoS_2 growth by chemical vapor deposition. *Nano Lett.* **2014**, *14* (2), 464−472.
(40) Park, J. H.; Lu, A. Y.; Shen, P. C.; Shin, B. G.; Wang, H.; Mao, N.; Xu, R.; Jung, S. J.; Ham, D.; Kern, K.; Han, Y.; Kong, J. Synthesis of high-performance monolayer molybdenum disulfide at low temperature. *Small Methods* **2021**, *5* (6), No. 2000720.
(41) Liu, B.; Fathi, M.; Chen, L.; Abbas, A.; Ma, Y.; Zhou, C. Chemical vapor deposition growth of monolayer WSe_2 with tunable device characteristics and growth mechanism study. *ACS Nano* **2015**, *9* (6), 6119−6127.
(42) Wang, S.; Rong, Y.; Fan, Y.; Pacios, M.; Bhaskaran, H.; He, K.; Warner, J. H. Shape evolution of monolayer MoS_2 crystals grown by chemical vapor deposition. *Chem. Mater.* **2014**, *26* (22), 6371−6379.
(43) Wang, X.; Zhang, Y. P.; Chen, Z. Q. Effect of MoO_3 constituents on the growth of MoS_2 nanosheets by chemical vapor deposition. *Mater. Res. Express.* **2016**, *3* (6), No. 065014.
(44) Wang, Q.; Shi, R.; Zhao, Y.; Huang, R.; Wang, Z.; Amini, A.; Cheng, C. Recent progress on kinetic control of chemical vapor deposition growth of high-quality wafer-scale transition metal dichalcogenides. *Nanoscale Adv.* **2021**, *3* (12), 3430−3440.
(45) Gao, Y.; Hong, Y. L.; Yin, L. C.; Wu, Z.; Yang, Z.; Chen, M. L.; Liu, Z.; Ma, T.; Sun, D. M.; Ni, Z.; Ma, X. L.; Cheng, H. M.; Ren, W. Ultrafast growth of high-quality monolayer WSe_2 on Au. *Adv. Mater.* **2017**, *29* (29), 1700990.
(46) Mandyam, S. V.; Kim, H. M.; Drndić, M. Large area few-layer TMD film growths and their applications. *J.Phys. Mater.* **2020**, *3* (2), No. 024008.
(47) Yang, P.; Zhang, S.; Pan, S.; Tang, B.; Liang, Y.; Zhao, X.; Zhang, Z.; Shi, J.; Huan, Y.; Shi, Y.; Pennycook, S. J.; Ren, Z.; Zhang, G.; Chen, Q.; Zou, X.; Liu, Z.; Zhang, Y. Epitaxial growth of centimeter-scale single-crystal MoS_2 monolayer on Au (111). *ACS Nano* **2020**, *14* (4), 5036−5045.
(48) Chen, J.; Zhao, X.; Tan, S. J.; Xu, H.; Wu, B.; Liu, B.; Fu, D.; Fu, W.; Geng, D.; Liu, Y.; Liu, W.; Tang, W.; Li, L.; Zhou, W.; Sum, T. C.; Loh, K. P. Chemical vapor deposition of large-size monolayer $MoSe_2$ crystals on molten glass. *J. Am. Chem. Soc.* **2017**, *139* (3), 1073−1076.
(49) Wang, S.; Pacios, M.; Bhaskaran, H.; Warner, J. H. Substrate control for large area continuous films of monolayer MoS_2 by atmospheric pressure chemical vapor deposition. *Nanotechnology* **2016**, *27* (8), No. 085604.
(50) Sial, M. N.; Usman, M.; Zheng, B.; Yu, Y.; Mavrič, A.; Qing, F.; Valant, M.; Wang, Z. M. CVD growth of molybdenum diselenide surface structures with tailored morphology. *CrystEngComm* **2018**, *20* (33), 4867−4874.

https://doi.org/10.1021/acsmaterialsau.2c00029
ACS Mater. Au 2022, 2, 665−685

(51) Gong, Y.; Zhang, X.; Redwing, J. M.; Jackson, T. N. Thin film transistors using wafer-scale low-temperature MOCVD WSe_2. *J. Electron. Mater.* **2016**, *45* (12), 6280−6284.
(52) Mun, J.; Park, H.; Park, J.; Joung, D.; Lee, S.-K.; Leem, J.; Myoung, J.-M.; Park, J.; Jeong, S.-H.; Chegal, W.; Nam, S.; Kang, S.-W. High-mobility MoS_2 directly grown on polymer substrate with kinetics-controlled metal−organic chemical vapor deposition. *ACS Appl. Electron. Mater.* **2019**, *1* (4), 608−616.
(53) Xu, X.; Yao, W.; Xiao, D.; Heinz, T. F. Spin and pseudospins in layered transition metal dichalcogenides. *Nat. Phys.* **2014**, *10* (5), 343−350.
(54) Wang, J.; Xu, X.; Cheng, T.; Gu, L.; Qiao, R.; Liang, Z.; Ding, D.; Hong, H.; Zheng, P.; Zhang, Z.; Zhang, Z.; Zhang, S.; Cui, G.; Chang, C.; Huang, C.; Qi, J.; Liang, J.; Liu, C.; Zuo, Y.; Xue, G.; Fang, X.; Tian, J.; Wu, M.; Guo, Y.; Yao, Z.; Jiao, Q.; Liu, L.; Gao, P.; Li, Q.; Yang, R.; Zhang, G.; Tang, Z.; Yu, D.; Wang, E.; Lu, J.; Zhao, Y.; Wu, S.; Ding, F.; Liu, K. Dual-coupling-guided epitaxial growth of wafer-scale single-crystal WS_2 monolayer on vicinal a-plane sapphire. *Nat. Nanotechnol.* **2022**, *17* (1), 33−38.
(55) Li, T.; Guo, W.; Ma, L.; Li, W.; Yu, Z.; Han, Z.; Gao, S.; Liu, L.; Fan, D.; Wang, Z.; Yang, Y.; Lin, W.; Luo, Z.; Chen, X.; Dai, N.; Tu, X.; Pan, D.; Yao, Y.; Wang, P.; Nie, Y.; Wang, J.; Shi, Y.; Wang, X. Epitaxial growth of wafer-scale molybdenum disulfide semiconductor single crystals on sapphire. *Nat. Nanotechnol.* **2021**, *16* (11), 1201−1207.
(56) Ruzmetov, D.; Zhang, K.; Stan, G.; Kalanyan, B.; Bhimanapati, G. R.; Eichfeld, S. M.; Burke, R. A.; Shah, P. B.; O'Regan, T. P.; Crowne, F. J.; Birdwell, A. G.; Robinson, J. A.; Davydov, A. V.; Ivanov, T. G. Vertical 2D/3D Semiconductor Heterostructures Based on Epitaxial Molybdenum Disulfide and Gallium Nitride. *ACS Nano* **2016**, *10* (3), 3580−3588.
(57) Aljarb, A.; Fu, J. H.; Hsu, C. C.; Chuu, C. P.; Wan, Y.; Hakami, M.; Naphade, D. R.; Yengel, E.; Lee, C. J.; Brems, S.; Chen, T. A.; Li, M. Y.; Bae, S. H.; Hsu, W. T.; Cao, Z.; Albaridy, R.; Lopatin, S.; Chang, W. H.; Anthopoulos, T. D.; Kim, J.; Li, L. J.; Tung, V. Ledge-directed epitaxy of continuously self-aligned single-crystalline nanoribbons of transition metal dichalcogenides. *Nat. Mater.* **2020**, *19* (12), 1300−1306.
(58) Yang, P.; Zou, X.; Zhang, Z.; Hong, M.; Shi, J.; Chen, S.; Shu, J.; Zhao, L.; Jiang, S.; Zhou, X.; Huan, Y.; Xie, C.; Gao, P.; Chen, Q.; Zhang, Q.; Liu, Z.; Zhang, Y. Batch production of 6-in. uniform monolayer molybdenum disulfide catalyzed by sodium in glass. *Nat. Commun.* **2018**, *9* (1), 979.
(59) Feijó, T. O.; Copetti, G.; Gerling, E. R. F.; Hanke, M.; Lopes, J. M. J.; Radtke, C.; Soares, G. V. The role of substrate on the growth of 2D heterostructures by CVD. *Appl. Surf. Sci.* **2021**, *539*, 148226.
(60) Wang, Q.; Li, N.; Tang, J.; Zhu, J.; Zhang, Q.; Jia, Q.; Lu, Y.; Wei, Z.; Yu, H.; Zhao, Y.; Guo, Y.; Gu, L.; Sun, G.; Yang, W.; Yang, R.; Shi, D.; Zhang, G. Wafer-scale highly oriented monolayer MoS_2 with large domain sizes. *Nano Lett.* **2020**, *20* (10), 7193−7199.
(61) Tong, X.; Liu, K.; Zeng, M.; Fu, L. Vapor-phase growth of high-quality wafer-scale two-dimensional materials. *InfoMat* **2019**, *1* (4), 460−478.
(62) Cheng, J.; Shen, C.; He, Y.; Wei, H.; Liu, S.; Qiu, P.; Song, Y.; Wei, S.; Wang, Z.; Zheng, X.; Peng, M. Reaction mechanism transformation of LPCVD-grown MoS_2 from isolated triangular grains to continuous films. *J. Alloys Compd.* **2021**, *853*, 157374.
(63) Ji, Q.; Kan, M.; Zhang, Y.; Guo, Y.; Ma, D.; Shi, J.; Sun, Q.; Chen, Q.; Zhang, Y.; Liu, Z. Unravelling orientation distribution and merging behavior of monolayer MoS_2 domains on sapphire. *Nano Lett.* **2015**, *15* (1), 198−205.
(64) Maury, F. Recent trends in the selection of metal-organic precursors for MOCVD process. *J. Phys. IV* **1995**, *5* (C5), 449−463.
(65) Schaefer, C. M.; Caicedo Roque, J. M.; Sauthier, G.; Bousquet, J.; Hébert, C.; Sperling, J. R.; Pérez-Tomás, A.; Santiso, J.; del Corro, E.; Garrido, J. A. Carbon incorporation in MOCVD of MoS_2 thin films grown from an organosulfide precursor. *Chem. Mater.* **2021**, *33* (12), 4474−4487.
(66) Kalanyan, B.; Kimes, W. A.; Beams, R.; Stranick, S. J.; Garratt, E.; Kalish, I.; Davydov, A. V.; Kanjolia, R. K.; Maslar, J. E. Rapid wafer-scale growth of polycrystalline 2H-MoS_2 by pulsed metal−organic chemical vapor deposition. *Chem. Mater.* **2017**, *29* (15), 6279−6288.
(67) Eichfeld, S. M.; Colon, V. O.; Nie, Y.; Cho, K.; Robinson, J. A. Controlling nucleation of monolayer WSe_2 during metal-organic chemical vapor deposition growth. *2D Mater.* **2016**, *3* (2), No. 025015.
(68) Zhang, K.; Bersch, B. M.; Zhang, F.; Briggs, N. C.; Subramanian, S.; Xu, K.; Chubarov, M.; Wang, K.; Lerach, J. O.; Redwing, J. M.; Fullerton-Shirey, S. K.; Terrones, M.; Robinson, J. A. Considerations for utilizing sodium chloride in epitaxial molybdenum disulfide. *ACS Appl. Mater. Interfaces* **2018**, *10* (47), 40831−40837.
(69) Chubarov, M.; Choudhury, T. H.; Hickey, D. R.; Bachu, S.; Zhang, T.; Sebastian, A.; Bansal, A.; Zhu, H.; Trainor, N.; Das, S.; Terrones, M.; Alem, N.; Redwing, J. M. Wafer-scale epitaxial growth of unidirectional WS_2 monolayers on sapphire. *ACS Nano* **2021**, *15* (2), 2532−2541.
(70) Bersch, B. M.; Eichfeld, S. M.; Lin, Y.-C.; Zhang, K.; Bhimanapati, G. R.; Piasecki, A. F.; Labella, M.; Robinson, J. A. Selective-area growth and controlled substrate coupling of transition metal dichalcogenides. *2D Mater.* **2017**, *4* (2), No. 025083.
(71) Zhang, T.; Li, Y.; Zhang, Y.; Feng, Q.; Ning, J.; Zhang, C.; Zhang, J.; Hao, Y. Investigation of β-Ga_2O_3 thin films grown on epi-GaN/sapphire (0001) substrates by low pressure MOCVD. *J. Alloys Compd.* **2021**, *859*, 157810.
(72) Michau, A.; Maury, F.; Schuster, F.; Boichot, R.; Pons, M.; Monsifrot, E. Chromium carbide growth at low temperature by a highly efficient DLI-MOCVD process in effluent recycling mode. *Surf. Coat. Technol.* **2017**, *332*, 96−104.
(73) Akiyama, K.; Nojima, S.; Takahashi, R.; Matsumoto, Y.; Funakubo, H. MOCVD growth of β-$FeSi_2$ film on modified Si surface by silver and enhancement of luminescence. *J. Cryst. Growth* **2019**, *506*, 131−134.
(74) Kang, K.; Xie, S.; Huang, L.; Han, Y.; Huang, P. Y.; Mak, K. F.; Kim, C.-J.; Muller, D.; Park, J. High-mobility three-atom-thick semiconducting films with wafer-scale homogeneity. *Nature* **2015**, *520* (7549), 656−660.
(75) Koma, A. Van der Waals epitaxy—a new epitaxial growth method for a highly lattice-mismatched system. *Thin Solid Films* **1992**, *216* (1), 72−76.
(76) Li, B.; Huang, L.; Zhong, M.; Li, Y.; Wang, Y.; Li, J.; Wei, Z. Direct vapor phase growth and optoelectronic application of large band offset SnS_2/MoS_2 vertical bilayer heterostructures with high lattice mismatch. *Adv. Electron. Mater.* **2016**, *2* (11), 1600298.
(77) Biroju, R. K.; Pal, S.; Sharma, R.; Giri, P.; Narayanan, T. N. Stacking sequence dependent photo-electrocatalytic performance of CVD grown MoS_2/graphene van der Waals solids. *Nanotechnology* **2017**, *28* (8), No. 085101.
(78) Paradisanos, I.; McCreary, K. M.; Adinehloo, D.; Mouchliadis, L.; Robinson, J. T.; Chuang, H.-J.; Hanbicki, A. T.; Perebeinos, V.; Jonker, B. T.; Stratakis, E.; Kioseoglou, G. Prominent room temperature valley polarization in WS_2/graphene heterostructures grown by chemical vapor deposition. *Appl. Phys. Lett.* **2020**, *116* (20), 203102.
(79) Wang, Y.-Y.; Chen, D.-R.; Wu, J.-K.; Wang, T.-H.; Chuang, C.; Huang, S.-Y.; Hsieh, W.-P.; Hofmann, M.; Chang, Y.-H.; Hsieh, Y.-P. Two-dimensional mechano-thermoelectric heterojunctions for self-powered strain sensors. *Nano Lett.* **2021**, *21* (16), 6990−6997.
(80) Zhang, Z.; Ji, X.; Shi, J.; Zhou, X.; Zhang, S.; Hou, Y.; Qi, Y.; Fang, Q.; Ji, Q.; Zhang, Y.; Hong, M.; Yang, P.; Liu, X.; Zhang, Q.; Liao, L.; Jin, C.; Liu, Z.; Zhang, Y. Direct chemical vapor deposition growth and band-gap characterization of MoS_2/h-BN van der Waals heterostructures on Au foils. *ACS Nano* **2017**, *11* (4), 4328−4336.
(81) Okada, M.; Sawazaki, T.; Watanabe, K.; Taniguch, T.; Hibino, H.; Shinohara, H.; Kitaura, R. Direct chemical vapor deposition growth of WS_2 atomic layers on hexagonal boron nitride. *ACS Nano* **2014**, *8* (8), 8273−8277.

https://doi.org/10.1021/acsmaterialsau.2c00029
ACS Mater. Au 2022, 2, 665−685

(82) Erkılıç, U.; Solís-Fernández, P.; Ji, H. G.; Shinokita, K.; Lin, Y.-C.; Maruyama, M.; Suenaga, K.; Okada, S.; Matsuda, K.; Ago, H. Vapor phase selective growth of two-dimensional perovskite/WS_2 heterostructures for optoelectronic applications. *ACS Appl. Mater. Interfaces* **2019**, *11* (43), 40503−40511.
(83) Guan, W.; Li, Y.; Zhong, Q.; Liu, H.; Chen, J.; Hu, H.; Lv, K.; Gong, J.; Xu, Y.; Kang, Z.; Cao, M.; Zhang, Q. Fabricating $MAPbI_3$/MoS_2 composites for improved photocatalytic performance. *Nano Lett.* **2021**, *21* (1), 597−604.
(84) Ai, R.; Guan, X.; Li, J.; Yao, K.; Chen, P.; Zhang, Z.; Duan, X.; Duan, X. Growth of single-crystalline cadmium iodide nanoplates, CdI_2/MoS_2 (WS_2, WSe_2) van der Waals heterostructures, and patterned arrays. *ACS Nano* **2017**, *11* (3), 3413−3419.
(85) Zheng, W.; Zheng, B.; Yan, C.; Liu, Y.; Sun, X.; Qi, Z.; Yang, T.; Jiang, Y.; Huang, W.; Fan, P.; Jiang, F.; Ji, W.; Wang, X.; Pan, A. Direct vapor growth of 2D vertical heterostructures with tunable band alignments and interfacial charge transfer behaviors. *Adv. Sci. (Weinh)* **2019**, *6* (7), 1802204.
(86) Rasmussen, F. A.; Thygesen, K. S. Computational 2D materials database: electronic structure of transition-metal dichalcogenides and oxides. *J. Phys. Chem. C* **2015**, *119* (23), 13169−13183.
(87) Gong, Y.; Lin, J.; Wang, X.; Shi, G.; Lei, S.; Lin, Z.; Zou, X.; Ye, G.; Vajtai, R.; Yakobson, B. I.; Terrones, H.; Terrones, M.; Tay, B. K.; Lou, J.; Pantelides, S. T.; Liu, Z.; Zhou, W.; Ajayan, P. M. Vertical and in-plane heterostructures from WS_2/MoS_2 monolayers. *Nat. Mater.* **2014**, *13* (12), 1135−42.
(88) Gong, Y.; Lei, S.; Ye, G.; Li, B.; He, Y.; Keyshar, K.; Zhang, X.; Wang, Q.; Lou, J.; Liu, Z.; Vajtai, R.; Zhou, W.; Ajayan, P. M. Two-step growth of two-dimensional WSe_2/$MoSe_2$ heterostructures. *Nano Lett.* **2015**, *15* (9), 6135−6141.
(89) Zhang, X.; Xiao, S.; Nan, H.; Mo, H.; Wan, X.; Gu, X.; Ostrikov, K. K. Controllable one-step growth of bilayer MoS_2−WS_2/WS_2 heterostructures by chemical vapor deposition. *Nanotechnology* **2018**, *29* (45), 455707.
(90) Fu, Q.; Wang, X.; Zhou, J.; Xia, J.; Zeng, Q.; Lv, D.; Zhu, C.; Wang, X.; Shen, Y.; Li, X.; Hua, Y.; Liu, F.; Shen, Z.; Jin, C.; Liu, Z. One-step synthesis of metal/semiconductor heterostructure NbS_2/MoS_2. *Chem. Mater.* **2018**, *30* (12), 4001−4007.
(91) Zhang, T.; Jiang, B.; Xu, Z.; Mendes, R. G.; Xiao, Y.; Chen, L.; Fang, L.; Gemming, T.; Chen, S.; Rummeli, M. H.; Fu, L. Twinned growth behaviour of two-dimensional materials. *Nat. Commun.* **2016**, *7* (1), 13911.
(92) Ding, Y.; Zhou, N.; Gan, L.; Yan, X.; Wu, R.; Abidi, I. H.; Waleed, A.; Pan, J.; Ou, X.; Zhang, Q.; Zhuang, M.; Wang, P.; Pan, X.; Fan, Z.; Zhai, T.; Luo, Z. Stacking-mode confined growth of 2H-$MoTe_2$/MoS_2 bilayer heterostructures for UV−vis−IR photodetectors. *Nano Energy* **2018**, *49*, 200−208.
(93) Heo, H.; Sung, J. H.; Jin, G.; Ahn, J. H.; Kim, K.; Lee, M. J.; Cha, S.; Choi, H.; Jo, M. H. Rotation-misfit-free heteroepitaxial stacking and stitching growth of hexagonal transition-metal dichalcogenide monolayers by nucleationkinetics controls. *Adv. Mater.* **2015**, *27* (25), 3803−3810.
(94) Yoo, Y.; Degregorio, Z. P.; Johns, J. E. Seed crystal homogeneity controls lateral and vertical heteroepitaxy of monolayer MoS_2 and WS_2. *J. Am. Chem. Soc.* **2015**, *137* (45), 14281−14287.
(95) Wu, X.; Wang, X.; Li, H.; Zeng, Z.; Zheng, B.; Zhang, D.; Li, F.; Zhu, X.; Jiang, Y.; Pan, A. Vapor growth of WSe_2/WS_2 heterostructures with stacking dependent optical properties. *Nano Res.* **2019**, *12* (12), 3123−3128.
(96) Zhang, Z.; Gong, Y.; Zou, X.; Liu, P.; Yang, P.; Shi, J.; Zhao, L.; Zhang, Q.; Gu, L.; Zhang, Y. Epitaxial growth of two-dimensional metal−semiconductor transition-metal dichalcogenide vertical stacks (VSe_2/MX_2) and their band alignments. *ACS Nano* **2019**, *13* (1), 885−893.
(97) Gong, X.; Zhao, X.; Pam, M. E.; Yao, H.; Li, Z.; Geng, D.; Pennycook, S. J.; Shi, Y.; Yang, H. Y. Location-selective growth of two-dimensional metallic/semiconducting transition metal dichalcogenide heterostructures. *Nanoscale* **2019**, *11* (10), 4183−4189.
(98) Yao, J.; Liu, H.; He, Q.; Chen, K.; Wu, Y.; Li, X.; Zhang, C.; Wu, Z.; Kang, J. Controllable growth of 2H-1T' MoS_2/ReS_2 heterostructures via chemical vapor deposition. *Appl. Surf. Sci.* **2022**, *572*, 151438.
(99) Liu, Z.; Feng, S.; Cai, X.; Liu, H.; Li, J.; Amjadian, M.; Cai, Y.; Wong, H.; Tamtaji, M.; An, L.; Zhang, K.; Chen, G.; Wang, N.; Xu, Z.; Luo, Z. Large-size superlattices synthesized by sequential sulfur substitution-induced transformation of metastable $MoTe_2$. *Chem. Mater.* **2021**, *33* (24), 9760−9768.
(100) Li, M. Y.; Shi, Y.; Cheng, C. C.; Lu, L. S.; Lin, Y. C.; Tang, H. L.; Tsai, M. L.; Chu, C. W.; Wei, K. H.; He, J. H.; Chang, W. H.; Suenaga, K.; Li, L. J. Epitaxial growth of a monolayer WSe_2-MoS_2 lateral p−n junction with an atomically sharp interface. *Science* **2015**, *349* (6247), 524−8.
(101) Huang, C.; Wu, S.; Sanchez, A. M.; Peters, J. J.; Beanland, R.; Ross, J. S.; Rivera, P.; Yao, W.; Cobden, D. H.; Xu, X. Lateral heterojunctions within monolayer $MoSe_2$−WSe_2 semiconductors. *Nat. Mater.* **2014**, *13* (12), 1096−1101.
(102) Gong, Y.; Lin, J.; Wang, X.; Shi, G.; Lei, S.; Lin, Z.; Zou, X.; Ye, G.; Vajtai, R.; Yakobson, B. I.; Terrones, H.; Terrones, M.; Tay, B. K.; Lou, J.; Pantelides, S. T.; Liu, Z.; Zhou, W.; Ajayan, P. M. Vertical and in-plane heterostructures from WS_2/MoS_2 monolayers. *Nat. Mater.* **2014**, *13* (12), 1135−1142.
(103) Wu, W.; Zhang, Q.; Zhou, X.; Li, L.; Su, J.; Wang, F.; Zhai, T. Self-powered photovoltaic photodetector established on lateral monolayer MoS_2-WS_2 heterostructures. *Nano Energy* **2018**, *51*, 45−53.
(104) Tsai, T.-H.; Liang, Z.-Y.; Lin, Y.-C.; Wang, C.-C.; Lin, K.-I.; Suenaga, K.; Chiu, P.-W. Photogating WS_2 photodetectors using embedded WSe_2 charge puddles. *ACS Nano* **2020**, *14* (4), 4559−4566.
(105) Duan, X.; Wang, C.; Shaw, J. C.; Cheng, R.; Chen, Y.; Li, H.; Wu, X.; Tang, Y.; Zhang, Q.; Pan, A.; Jiang, J.; Yu, R.; Huang, Y.; Duan, X. Lateral epitaxial growth of two-dimensional layered semiconductor heterojunctions. *Nat. Nanotechnol.* **2014**, *9* (12), 1024−1030.
(106) Bogaert, K.; Liu, S.; Chesin, J.; Titow, D.; Gradecak, S.; Garaj, S. Diffusion-mediated synthesis of MoS_2/WS_2 lateral heterostructures. *Nano Lett.* **2016**, *16* (8), 5129−5134.
(107) Zhang, X.-Q.; Lin, C.-H.; Tseng, Y.-W.; Huang, K.-H.; Lee, Y.-H. Synthesis of lateral heterostructures of semiconducting atomic layers. *Nano Lett.* **2015**, *15* (1), 410−415.
(108) Li, L.; Zheng, W.; Ma, C.; Zhao, H.; Jiang, F.; Ouyang, Y.; Zheng, B.; Fu, X.; Fan, P.; Zheng, M.; Li, Y.; Xiao, Y.; Cao, W.; Jiang, Y.; Zhu, X.; Zhuang, X.; Pan, A. Wavelength-tunable interlayer exciton emission at the near-infrared region in van der Waals semiconductor heterostructures. *Nano Lett.* **2020**, *20* (5), 3361−3368.
(109) Zheng, B.; Ma, C.; Li, D.; Lan, J.; Zhang, Z.; Sun, X.; Zheng, W.; Yang, T.; Zhu, C.; Ouyang, G.; Xu, G.; Zhu, X.; Wang, X.; Pan, A. Band alignment engineering in two-dimensional lateral heterostructures. *J. Am. Chem. Soc.* **2018**, *140* (36), 11193−11197.
(110) Sahoo, P. K.; Memaran, S.; Xin, Y.; Balicas, L.; Gutiérrez, H. R. One-pot growth of two-dimensional lateral heterostructures via sequential edge-epitaxy. *Nature* **2018**, *553* (7686), 63−67.
(111) Tsai, T.-H.; Liang, Z.-Y.; Lin, Y.-C.; Wang, C.-C.; Lin, K.-I.; Suenaga, K.; Chiu, P.-W. Photogating WS_2 photodetectors using embedded WSe_2 charge puddles. *ACS Nano* **2020**, *14* (4), 4559−4560.
(112) Zhang, T.; Wang, Y.; Xu, J.; Chen, L.; Zhu, H.; Sun, Q.; Ding, S.; Zhang, D. W. High performance few-layer MoS_2 transistor arrays with wafer level homogeneity integrated by atomic layer deposition. *2D Mater.* **2018**, *5* (1), No. 015028.
(113) Seok, H.; Megra, Y. T.; Kanade, C. K.; Cho, J.; Kanade, V. K.; Kim, M.; Lee, I.; Yoo, P. J.; Kim, H. U.; Suk, J. W.; Kim, T. Low-temperature synthesis of wafer-scale MoS_2−WS_2 vertical heterostructures by single-step penetrative plasma sulfurization. *ACS Nano* **2021**, *15* (1), 707−718.
(114) Chen, J.; Shao, K.; Yang, W.; Tang, W.; Zhou, J.; He, Q.; Wu, Y.; Zhang, C.; Li, X.; Yang, X.; Wu, Z.; Kang, J. Synthesis of wafer-

https://doi.org/10.1021/acsmaterialsau.2c00029
ACS Mater. Au 2022, 2, 665−685

scale monolayer WS_2 crystals toward the application in integrated electronic devices. *ACS Appl. Mater. Interfaces* **2019**, *11* (21), 19381−19387.
(115) Wang, X.; Kang, K.; Chen, S.; Du, R.; Yang, E.-H. Location-specific growth and transfer of arrayed MoS_2 monolayers with controllable size. *2D Mater.* **2017**, *4* (2), No. 025093.
(116) Wang, X.; Wang, B.; Zhang, Q.; Sun, Y.; Wang, E.; Luo, H.; Wu, Y.; Gu, L.; Li, H.; Liu, K. Grain-boundary engineering of monolayer MoS_2 for energy-efficient lateral synaptic devices. *Adv. Mater.* **2021**, *33* (32), 2102435.
(117) Guimaraes, M. H. D.; Gao, H.; Han, Y.; Kang, K.; Xie, S.; Kim, C.-J.; Muller, D. A.; Ralph, D. C.; Park, J. Atomically thin ohmic edge contacts between two-dimensional materials. *ACS Nano* **2016**, *10* (6), 6392−6399.
(118) Kang, W. T.; Phan, T. L.; Ahn, K. J.; Lee, I.; Kim, Y. R.; Won, U. Y.; Kim, J. E.; Lee, Y. H.; Yu, W. J. Selective pattern growth of atomically thin $MoSe_2$ films via a surface-mediated liquid-phase pomoter. *ACS Appl. Mater. Interfaces* **2021**, *13* (15), 18056−18064.
(119) Zhou, X.; Tian, Z.; Kim, H. J.; Wang, Y.; Xu, B.; Pan, R.; Chang, Y. J.; Di, Z.; Zhou, P.; Mei, Y. Rolling up $MoSe_2$ nanomembranes as a sensitive tubular photodetector. *Small* **2019**, *15* (42), No. 1902528.
(120) Li, S.; Pam, M. E.; Li, Y.; Chen, L.; Chien, Y. C.; Fong, X.; Chi, D.; Ang, K. W. Wafer-scale 2D hafnium diselenide based memristor crossbar array for energy-efficient neural network hardware. *Adv. Mater.* **2022**, *34*, 2103376.
(121) Seol, M.; Lee, M. H.; Kim, H.; Shin, K. W.; Cho, Y.; Jeon, I.; Jeong, M.; Lee, H. I.; Park, J.; Shin, H. J. High-throughput growth of wafer-scale monolayer transition metal dichalcogenide via vertical ostwald pipening. *Adv. Mater.* **2020**, *32* (42), 2003542.
(122) Sangwan, V. K.; Lee, H. S.; Bergeron, H.; Balla, I.; Beck, M. E.; Chen, K. S.; Hersam, M. C. Multi-terminal memtransistors from polycrystalline monolayer molybdenum disulfide. *Nature* **2018**, *554* (7693), 500−504.
(123) Poddar, P. K.; Zhong, Y.; Mannix, A. J.; Mujid, F.; Yu, J.; Liang, C.; Kang, J.-H.; Lee, M.; Xie, S.; Park, J. Resist-free lithography for monolayer transition metal dichalcogenides. *Nano Lett.* **2022**, *22*, 726−732.
(124) Rho, Y.; Pei, J.; Wang, L.; Su, Z.; Eliceiri, M.; Grigoropoulos, C. P. Site-selective atomic layer precision thinning of MoS_2 via laser-assisted anisotropic chemical etching. *ACS Appl. Mater. Interfaces* **2019**, *11* (42), 39385−39393.
(125) Wang, P.; Song, S.; Najafi, A.; Huai, C.; Zhang, P.; Hou, Y.; Huang, S.; Zeng, H. High-fidelity transfer of chemical vapor deposition grown 2D transition metal dichalcogenides via substrate decoupling and polymer/small molecule composite. *ACS Nano* **2020**, *14* (6), 7370−7379.
(126) Meng, W.; Xu, F.; Yu, Z.; Tao, T.; Shao, L.; Liu, L.; Li, T.; Wen, K.; Wang, J.; He, L.; Sun, L.; Li, W.; Ning, H.; Dai, N.; Qin, F.; Tu, X.; Pan, D.; He, S.; Li, D.; Zheng, Y.; Lu, Y.; Liu, B.; Zhang, R.; Shi, Y.; Wang, X. Three-dimensional monolithic micro-LED display driven by atomically thin transistor matrix. *Nat. Nanotechnol.* **2021**, *16* (11), 1231−1236.
(127) Villaos, R. A. B.; Crisostomo, C. P.; Huang, Z.-Q.; Huang, S.-M.; Padama, A. A. B.; Albao, M. A.; Lin, H.; Chuang, F.-C. Thickness dependent electronic properties of Pt dichalcogenides. *npj 2D Mater. Appl.* **2019**, *3* (1), 2.
(128) Xue, Y.; Zhang, Y.; Liu, Y.; Liu, H.; Song, J.; Sophia, J.; Liu, J.; Xu, Z.; Xu, Q.; Wang, Z.; Zheng, J.; Liu, Y.; Li, S.; Bao, Q. Scalable production of a few-layer MoS_2/WS_2 vertical heterojunction array and its application for photodetectors. *ACS Nano* **2016**, *10* (1), 573−80.
(129) Woods, J. M.; Jung, Y.; Xie, Y.; Liu, W.; Liu, Y.; Wang, H.; Cha, J. J. One-step synthesis of MoS_2/WS_2 layered heterostructures and catalytic activity of defective transition metal dichalcogenide films. *ACS Nano* **2016**, *10* (2), 2004−2009.
(130) Dong, R.; Moore, L.; Ocola, L. E.; Kuljanishvili, I. Enabling quality interfaces with mask-free approach to selective growth of MoS_2/graphene stacked structures. *Adv. Funct. Inter.* **2016**, *3* (16), 1600098.
(131) Song, S.; Sim, Y.; Kim, S.-Y.; Kim, J. H.; Oh, I.; Na, W.; Lee, D. H.; Wang, J.; Yan, S.; Liu, Y.; Kwak, J.; Chen, J.-H.; Cheong, H.; Yoo, J.-W.; Lee, Z.; Kwon, S.-Y. Wafer-scale production of patterned transition metal ditelluride layers for two-dimensional metal−semiconductor contacts at the Schottky−Mott limit. *Nature Electronics* **2020**, *3* (4), 207−215.
(132) Son, S. B.; Kim, Y.; Kim, A.; Cho, B.; Hong, W.-K. Ultraviolet wavelength-dependent optoelectronic properties in two-dimensional $NbSe_2−WSe_2$ van der waals heterojunction-based field-effect transistors. *ACS Appl. Mater. Interfaces* **2017**, *9* (47), 41537−41545.
(133) Zhu, J.; Wang, Z.; Yu, H.; Li, N.; Zhang, J.; Meng, J.; Liao, M.; Zhao, J.; Lu, X.; Du, L.; Yang, R.; Shi, D.; Jiang, Y.; Zhang, G. Argon plasma induced phase transition in monolayer MoS_2. *J. Am. Chem. Soc.* **2017**, *139* (30), 10216−10219.
(134) Mahjouri-Samani, M.; Lin, M. W.; Wang, K.; Lupini, A. R.; Lee, J.; Basile, L.; Boulesbaa, A.; Rouleau, C. M.; Puretzky, A. A.; Ivanov, I. N.; Xiao, K.; Yoon, M.; Geohegan, D. B. Patterned arrays of lateral heterojunctions within monolayer two-dimensional semiconductors. *Nat. Commun.* **2015**, *6*, 7749.
(135) Afaneh, T.; Sahoo, P. K.; Nobrega, I. A.; Xin, Y.; Gutiérrez, H. R. Laser-assisted chemical modification of monolayer transition metal dichalcogenides. *Adv. Funct. Mater.* **2018**, *28* (37), 1802949.
(136) Wang, X.; Wang, B.; Wu, Y.; Wang, E.; Luo, H.; Sun, Y.; Fu, D.; Sun, Y.; Liu, K. Two-Dimensional Lateral Heterostructures Made by Selective Reaction on a Patterned Monolayer MoS2Matrix. *ACS Appl. Mater. Interfaces* **2021**, *13* (22), 26143−26151.
(137) Chen, X.; Park, Y. J.; Das, T.; Jang, H.; Lee, J.-B.; Ahn, J.-H. Lithography-free plasma-induced patterned growth of MoS_2 and its heterojunction with graphene. *Nanoscale* **2016**, *8* (33), 15181−15188.
(138) Zhang, K.; Ding, C.; Pan, B.; Wu, Z.; Marga, A.; Zhang, L.; Zeng, H.; Huang, S. Visualizing van der Waals epitaxial growth of 2D heterostructures. *Adv. Mater.* **2021**, *33* (45), 2105079.
(139) Mohapatra, P. K.; Ranganathan, K.; Ismach, A. Selective area growth and transfer of high optical quality MoS_2 layers. *Adv. Funct. Inter.* **2020**, *7* (24), 2001549.
(140) Wan, W.; Zhan, L.; Shih, T.-M.; Zhu, Z.; Lu, J.; Huang, J.; Zhang, Y.; Huang, H.; Zhang, X.; Cai, W. Controlled growth of MoS_2 via surface-energy alterations. *Nanotechnology* **2020**, *31* (3), No. 035601.
(141) Kim, H. J.; Kim, H.; Yang, S.; Kwon, J. Y. Grains in selectively grown MoS_2 thin films. *Small* **2017**, *13* (46), 1702256.
(142) Zhao, M.; Ye, Y.; Han, Y.; Xia, Y.; Zhu, H.; Wang, S.; Wang, Y.; Muller, D. A.; Zhang, X. Large-scale chemical assembly of atomically thin transistors and circuits. *Nat. Nanotechnol* **2016**, *11* (11), 954−959.
(143) Li, X.; Kahn, E.; Chen, G.; Sang, X.; Lei, J.; Passarello, D.; Oyedele, A. D.; Zakhidov, D.; Chen, K. W.; Chen, Y. X.; Hsieh, S. H.; Fujisawa, K.; Unocic, R. R.; Xiao, K.; Salleo, A.; Toney, M. F.; Chen, C. H.; Kaxiras, E.; Terrones, M.; Yakobson, B. I.; Harutyunyan, A. R. Surfactant-mediated growth and patterning of atomically thin transition metal dichalcogenides. *ACS Nano* **2020**, *14* (6), 6570−6581.
(144) Ryu, B.; Li, D.; Park, C.; Rokni, H.; Lu, W.; Liang, X. Rubbing-induced site-selective growth of MoS_2 device patterns. *ACS Appl. Mater. Interfaces* **2018**, *10* (50), 43774−43784.
(145) Ryu, B.; Yoon, J. S.; Kazyak, E.; Chen, K. H.; Park, Y.; Dasgupta, N. P.; Liang, X. Inkjet-defined site-selective (IDSS) growth for controllable production of in-plane and out-of-plane MoS_2 device arrays. *Nanoscale* **2020**, *12* (32), 16917−16927.
(146) Li, J.; Yang, X.; Liu, Y.; Huang, B.; Wu, R.; Zhang, Z.; Zhao, B.; Ma, H.; Dang, W.; Wei, Z.; Wang, K.; Lin, Z.; Yan, X.; Sun, M.; Li, B.; Pan, X.; Luo, J.; Zhang, G.; Liu, Y.; Huang, Y.; Duan, X.; Duan, X. General synthesis of two-dimensional van der Waals heterostructure arrays. *Nature* **2020**, *579* (7799), 368−374.
(147) Lee, G. H.; Yu, Y. J.; Cui, X.; Petrone, N.; Lee, C. H.; Choi, M. S.; Lee, D. Y.; Lee, C.; Yoo, W. J.; Watanabe, K.; Taniguchi, T.; Nuckolls, C.; Kim, P.; Hone, J. Flexible and transparent MoS_2 field-effect transistors on hexagonal boron nitride-graphene heterostructures. *ACS Nano* **2013**, *7* (9), 7931−6.

https://doi.org/10.1021/acsmaterialsau.2c00029
ACS Mater. Au 2022, 2, 665−685

(148) Feng, J.; Sun, X.; Wu, C.; Peng, L.; Lin, C.; Hu, S.; Yang, J.; Xie, Y. Metallic few-layered VS_2 ultrathin nanosheets: high two-dimensional conductivity for in-plane supercapacitors. *J. Am. Chem. Soc.* **2011**, *133* (44), 17832−17838.
(149) Li, N.; Wang, Q.; Shen, C.; Wei, Z.; Yu, H.; Zhao, J.; Lu, X.; Wang, G.; He, C.; Xie, L.; Zhu, J.; Du, L.; Yang, R.; Shi, D.; Zhang, G. Large-scale flexible and transparent electronics based on monolayer molybdenum disulfide field-effect transistors. *Nat. Electron.* **2020**, *3* (11), 711−717.
(150) Yu, Z.; Ong, Z. Y.; Li, S.; Xu, J. B.; Zhang, G.; Zhang, Y. W.; Shi, Y.; Wang, X. Analyzing the carrier mobility in transition-metal dichalcogenide MoS_2 field-effect transistors. *Adv. Funct. Mater.* **2017**, *27* (19), 1604093.
(151) Dushaq, G.; Rasras, M. Planar multilayered 2D GeAs schottky photodiode for high-performance visible−near-infrared photodetection. *ACS Appl. Mater. Interfaces* **2021**, *13* (18), 21499−21506.
(152) Duan, X.; Wang, C.; Fan, Z.; Hao, G.; Kou, L.; Halim, U.; Li, H.; Wu, X.; Wang, Y.; Jiang, J.; Pan, A.; Huang, Y.; Yu, R.; Duan, X. Synthesis of $WS_{2x}Se_{2-2x}$ alloy nanosheets with composition-tunable electronic properties. *Nano Lett.* **2016**, *16* (1), 264−9.
(153) Taghinejad, H.; Taghinejad, M.; Eftekhar, A. A.; Li, Z.; West, M. P.; Javani, M. H.; Abdollahramezani, S.; Zhang, X.; Tian, M.; Johnson-Averette, T.; Ajayan, P. M.; Vogel, E. M.; Shi, S. F.; Cai, W.; Adibi, A. Synthetic engineering of morphology and electronic band gap in lateral heterostructures of monolayer transition metal dichalcogenides. *ACS Nano* **2020**, *14* (5), 6323−6330.
(154) Johari, P.; Shenoy, V. B. Tuning the electronic properties of semiconducting transition metal dichalcogenides by applying mechanical strains. *ACS Nano* **2012**, *6* (6), 5449−5456.
(155) Lloyd, D.; Liu, X.; Christopher, J. W.; Cantley, L.; Wadehra, A.; Kim, B. L.; Goldberg, B. B.; Swan, A. K.; Bunch, J. S. Band gap engineering with ultralarge biaxial strains in suspended monolayer MoS_2. *Nano Lett.* **2016**, *16* (9), 5836−5841.
(156) Conley, H. J.; Wang, B.; Ziegler, J. I.; Haglund, R. F., Jr; Pantelides, S. T.; Bolotin, K. Bandgap engineering of strained monolayer and bilayer MoS_2. *Nano Lett.* **2013**, *13* (8), 3626−3630.
(157) Santos, E. J.; Kaxiras, E. Electrically driven tuning of the dielectric constant in MoS_2 layers. *ACS Nano* **2013**, *7* (12), 10741−10746.
(158) Habib, M. R.; Wang, S.; Wang, W.; Xiao, H.; Obaidulla, S. M.; Gayen, A.; Khan, Y.; Chen, H.; Xu, M. Electronic properties of polymorphic two-dimensional layered chromium disulphide. *Nanoscale* **2019**, *11* (42), 20123−20132.
(159) Lukman, S.; Ding, L.; Xu, L.; Tao, Y.; Riis-Jensen, A. C.; Zhang, G.; Wu, Q. Y. S.; Yang, M.; Luo, S.; Hsu, C.; Yao, L.; Liang, G.; Lin, H.; Zhang, Y. W.; Thygesen, K. S.; Wang, Q. J.; Feng, Y.; Teng, J. High oscillator strength interlayer excitons in two-dimensional heterostructures for mid-infrared photodetection. *Nat. Nanotechnol.* **2020**, *15* (8), 675−682.
(160) Hong, X.; Kim, J.; Shi, S.-F.; Zhang, Y.; Jin, C.; Sun, Y.; Tongay, S.; Wu, J.; Zhang, Y.; Wang, F. Ultrafast charge transfer in atomically thin MoS_2/WS_2 heterostructures. *Nat. Nanotechnol.* **2014**, *9* (9), 682−686.
(161) Britnell, L.; Ribeiro, R. M.; Eckmann, A.; Jalil, R.; Belle, B. D.; Mishchenko, A.; Kim, Y. J.; Gorbachev, R. V.; Georgiou, T.; Morozov, S. V.; Grigorenko, A. N.; Geim, A. K.; Casiraghi, C.; Castro Neto, A. H.; Novoselov, K. S. Strong light-matter interactions in heterostructures of atomically thin films. *Science* **2013**, *340* (6138), 1311−4.
(162) Kumar, A.; Ahluwalia, P. Electronic structure of transition metal dichalcogenides monolayers 1H-MX_2 (M= Mo, W; X= S, Se, Te) from ab-initio theory: new direct band gap semiconductors. *Eur.Phys. J. B* **2012**, *85* (6), 186.
(163) Huo, N.; Konstantatos, G. Recent progress and future prospects of 2D-based photodetectors. *Adv. Mater.* **2018**, *30* (51), 1801164.
(164) Yang, P.; Zou, X.; Zhang, Z.; Hong, M.; Shi, J.; Chen, S.; Shu, J.; Zhao, L.; Jiang, S.; Zhou, X. Batch production of 6-in. uniform monolayer molybdenum disulfide catalyzed by sodium in glass. *Nat. Commun.* **2018**, *9* (1), 979.
(165) Chen, J.; Zhao, X.; Tan, S. J. R.; Xu, H.; Wu, B.; Liu, B.; Fu, D.; Fu, W.; Geng, D.; Liu, Y.; Liu, W.; Tang, W.; Li, L.; Zhou, W.; Sum, T. C.; Loh, K. P. Chemical vapor deposition of large-size monolayer $MoSe_2$ crystals on molten glass. *J. Am. Chem. Soc.* **2017**, *139* (3), 1073−1076.
(166) Zhang, Z.; Liu, Y.; Dai, C.; Yang, X.; Chen, P.; Ma, H.; Zhao, B.; Wu, R.; Huang, Z.; Wang, D.; Liu, M.; Huangfu, Y.; Xin, S.; Luo, J.; Wang, Y.; Li, J.; Li, B.; Duan, X. Highly selective synthesis of monolayer or bilayer WSe_2 single crystals by pre-annealing the solid precursor. *Chem. Mater.* **2021**, *33* (4), 1307−1313.
(167) Xu, X.; Chen, S.; Liu, S.; Cheng, X.; Xu, W.; Li, P.; Wan, Y.; Yang, S.; Gong, W.; Yuan, K.; Gao, P.; Ye, Y.; Dai, L. Millimeter-scale single-crystalline semiconducting $MoTe_2$ via solid-to-solid phase transformation. *J. Am. Chem. Soc.* **2019**, *141* (5), 2128−2134.
(168) Najafidehaghani, E.; Gan, Z.; George, A.; Lehnert, T.; Ngo, G. Q.; Neumann, C.; Bucher, T.; Staude, I.; Kaiser, D.; Vogl, T.; Hübner, U.; Kaiser, U.; Eilenberger, F.; Turchanin, A. 1D p−n junction electronic and optoelectronic devices from transition metal dichalcogenide lateral heterostructures grown by one-pot chemical vapor deposition synthesis. *Adv. Funct. Mater.* **2021**, *31* (27), 2101086.
(169) Leong, W. S.; Ji, Q.; Mao, N.; Han, Y.; Wang, H.; Goodman, A. J.; Vignon, A.; Su, C.; Guo, Y.; Shen, P. C.; Gao, Z.; Muller, D. A.; Tisdale, W. A.; Kong, J. Synthetic lateral metal-semiconductor heterostructures of transition metal disulfides. *J. Am. Chem. Soc.* **2018**, *140* (39), 12354−12358.
(170) Nasr, J. R.; Simonson, N.; Oberoi, A.; Horn, M. W.; Robinson, J. A.; Das, S. Low-power and ultra-thin MoS_2 photodetectors on glass. *ACS Nano* **2020**, *14* (11), 15440−15449.
(171) Zhu, J.; Li, W.; Huang, R.; Ma, L.; Sun, H.; Choi, J.-H.; Zhang, L.; Cui, Y.; Zou, G. One-pot selective epitaxial growth of large WS_2/MoS_2 lateral and vertical heterostructures. *J. Am. Chem. Soc.* **2020**, *142* (38), 16276−16284.
(172) Xia, J.; Yan, J.; Wang, Z.; He, Y.; Gong, Y.; Chen, W.; Sum, T. C.; Liu, Z.; Ajayan, P. M.; Shen, Z. Strong coupling and pressure engineering in WSe_2-$MoSe_2$ heterobilayers. *Nat. Phys.* **2021**, *17* (1), 92−98.
(173) Yuan, L.; Zheng, B.; Kunstmann, J.; Brumme, T.; Kuc, A. B.; Ma, C.; Deng, S.; Blach, D.; Pan, A.; Huang, L. Twist-angle-dependent interlayer exciton diffusion in WS_2−WSe_2 heterobilayers. *Nat. Mater.* **2020**, *19* (6), 617−624.
(174) Wu, R.; Tao, Q.; Dang, W.; Liu, Y.; Li, B.; Li, J.; Zhao, B.; Zhang, Z.; Ma, H.; Sun, G.; Duan, X.; Duan, X. van der Waals epitaxial growth of atomically thin 2D metals on dangling-bond-free WSe_2 and WS_2. *Adv. Funct. Mater.* **2019**, *29* (12), 1806611.
(175) Li, B.; Wan, Z.; Wang, C.; Chen, P.; Huang, B.; Cheng, X.; Qian, Q.; Li, J.; Zhang, Z.; Sun, G.; Zhao, B.; Ma, H.; Wu, R.; Wei, Z.; Liu, Y.; Liao, L.; Ye, Y.; Huang, Y.; Xu, X.; Duan, X.; Ji, W.; Duan, X. Van der Waals epitaxial growth of air-stable $CrSe_2$ nanosheets with thickness-tunable magnetic order. *Nat. Mater.* **2021**, *20* (6), 818−825.

https://doi.org/10.1021/acsmaterialsau.2c00029
ACS Mater. Au 2022, 2, 665−685